Physics of the Earth and Planetary Interiors 309 (2020) 106603

Contents lists available at ScienceDirect

Physics of the Earth and Planetary Interiors

journal homepage: www.elsevier.com/locate/pepi

Simulation of Strong Ground Motion for an Mw 7.0 Earthquake beneath the Bhutan Himalaya in NE India and its trans-boundary seismic hazard implications

Babita Sharma, O.P. Mishra *

National Centre for Seismology, Ministry of Earth Sciences, New Delhi, India

ARTICLE INFO

Keywords:
Strong ground motion
Trans-boundary earthquake
Rupture location
Rupture directivity
Earthquake hazards

ABSTRACT

We simulate the strong ground motion for an expected major earthquake (Mw 7.0) beneath the Bhutan Himalayan region with an empirical Green's function method using waveforms recorded from the 2009 Bhutan mainshock (Mw 6.1) and its largest aftershock (Mw 5.1). Fault orientation and location of the simulated event extend the length of the fault plane determined from the 2009 Bhutan mainshock and aftershock along its strike. The simulated PGA values are compared with the results derived from a ground motion prediction equation (GMPE) for the Himalayan region and it is found that different levels of accelerations are associated with different rupture initiation points on the fault plane. It is observed that the NE Indian region is capable of generating peak ground acceleration (PGA) in exceedance to 121 cm/s^2 for simulated earthquake (Mw 7.0). The maximum impacts of shaking will be on the sites located near the rupture initiation points that are poised to generate higher values of ground acceleration. To validate our simulation, we also estimate the extent of rupture directivity of the simulated earthquake with respect to four initiation points indicating that higher value of PGA and shaking duration exist either to South or to South-West azimuths from the imitated locations, which are corroborated with respective geology of the sites. This study suggests that areas of maximum ground shaking would occur in the vicinity of the source initiation where possibility of relatively stronger earthquake hazards does exist, which in turn requires attention for adoption of earthquake risk mitigation plans in view of impacts of trans-boundary earthquakes in the region.

1. Introduction

The Indian subcontinent is experiencing the collision of the Indian plate with the Eurasian plate and associated with seismogenesis because of crustal dynamical processes and changes in strain energy (Tapponnier et al., 1981; 1990; England and Houseman, 1986; Yin and Harrison, 2000; He et al., 2018). Due to this activity, the inter-plate region of the Himalayan arc from west to east is seismically active (Searle et al., 1987). The Himalayan arc has witnessed several destructive earthquakes in 19th and 20th centuries like the 1897 Shillong earthquake (*M* 8.1), the 1905 Kangra earthquake (*M* 7.8), the 1934 Bihar-Nepal earthquake (*M* 8.4), and the 1950 Assam earthquake (*M* 8.7). These earthquakes produced significant loss of human lives and property in the Himalayan and its surrounding regions (Bilham, 2004; Kayal, 2008). Recently, two major earthquakes, the 2005 Kashmir earthquake (M_w 7.6) and the 2015 Gorkha earthquake (M_w 7.8), occurred in the detachment zone of the thrusting Indian plate demonstrating the tendency of Himalayan arc to produce disastrous earthquakes.

The recurrence of similar or larger earthquakes has been the most debated issue in the Himalayan arc region and its adjacent areas because of intricate seismotectonic settings of the region (Mishra, 2014). The activity related to the under-thrusting of the Indian Plate beneath the Tibetan Plateau is the causative source of occurrence of earthquakes in the entire Himalayan arc, which has sufficient contrasts in structure heterogeneities in association with anisotropic variation in the physical property of the undergoing and over-ridding plate in the subduction-collisional tectonics as reported by several researchers, elsewhere in the world (Tapponnier et al., 1981; 1990; England and Houseman, 1986; Yin and Harrison, 2000; Lei et al., 2009; Mishra, 2014; Zhou and Lei, 2016; Lei and Zhao, 2016; He et al., 2018; Lei et al., 2019). Moreover, there are several seismic gaps in the Himalayan arc where active faults have not produced seismicity for long periods of time as compared to

* Corresponding author.
E-mail address: omp.mishra@nic.in (O.P. Mishra).

https://doi.org/10.1016/j.pepi.2020.106603
Received 20 July 2020; Received in revised form 29 October 2020; Accepted 31 October 2020
Available online 9 November 2020

other parts (Bilham and Wallace, 2005; Mishra, 2014). Bilham and Wallace (2005) have given the slip potential in comparison with population residing in plain areas for the entire Himalayan range which shows a dangerous situation over the densely populated areas due to the future probabilistic earthquakes in the Himalayan ranges. The seismic zonation map of India (Fig. 1, inset) given by the Bureau of Indian Standard (BIS, 2002), divides the country into four seismic zones, based on observations of past earthquakes and future probable earthquakes. It is important to note that the entire NE India falls under Zone V on the seismic hazard map, which is the most hazardous zone. Gupta and Gahalaut (2014) based on the GPS data, have also stated that the entire Himalayan arc is capable to generate the great earthquake. Based on geodetic studies, the possibility of a magnitude M_w 8.2–9.0 earthquake in the Indo-Burmese wedge has been discussed by Steckler et al. (2016). The matter of the fact is that the Bhutan region of Himalayan range in the NE India is accumulating stress due to the continuous motion of the Indian plate. Many investigations also have marked the idea that this region is the area of great concern having considerably low seismicity in the previous two centuries (Kayal, 2008; Bilham, 2004). It is also mentioned that the geodetic information in this part of Himalaya is sparse and the strain released from the past earthquakes shows scarce seismic moment computed geodetically (Bilham et al., 2001). The adjoining states of Indian subcontinent in this part are under the threat of futuristic probable strong ground motions which may be produced by the Bhutan Himalayan region. However, one moderate earthquake (M_w 6.2) in 2009 is the latest earthquake in this region which caused considerable damage in Bhutan and several cities of India in the border areas of India to Bhutan (Kayal, 2008; Le Roux-Mallouf et al., 2015).

Seismologists and earthquake engineers are very much interested to know details about the ground motion for the large earthquakes to understand how the geotectonic settings control the degree of earthquake shakings to cause seismic hazards in the region of high earthquake potentiality. This information, for various tectonic regions, is very scarce, as the instrumentation systems have been implemented after 1964 or possibly later in case of developing countries.

In this context, our simulation of strong ground motion for the Bhutan Himalaya would be helpful for assessing the ground motions of future probable earthquakes in a seismically active region, which has close correspondence to the source, path and site characteristics of the wave motion (Irikura et al., 1997; Dinesh et al., 1999; Sriram and Khattri, 1999; Sharma and Rastogi, 2014; Sharma et al., 2015; Mittal and Kumar, 2015; Sharma et al., 2016a). There are numerous available techniques for simulating strong ground motions and they are being used all over the world. These techniques include Green's function technique (Ordaz et al., 1995), stochastic technique (Motazedian and Atkinson, 2005) and hybrid technique (Kamae et al., 1998). The EGF technique, originally was proposed by Hartzell (1978), and later on the methodology was extended for broadband ground motions by Irikura (1983). After that this technique was again modified by Irikura (1986) and Irikura et al. (1997). EGF technique is very important, which uses original earthquake as an element earthquake because small earthquakes contain the information of the source, path & site. At the same location of the element earthquake, the target earthquake is simulated using various input parameters (Frankel, 1995; Irikura et al., 1997; Khattri, 1999; Ordaz et al., 1995; Singh et al., 2002). In the present study, we used the modified EGF method of Irikura et al. (1997) to simulate ground motion scenario for the NE India, which has a wide applicability in different tectonic zones used by different researchers, elsewhere in the world (Irikura et al., 1997; Singh et al., 2002; Sharma et al., 2013; Sharma et al., 2016a, 2016b). We also attempted to simulate earthquake ground motions using the Bhutan earthquake and its strongest aftershock recorded by strong motion accelerographs located in NE India (Fig. 2). This study is important to know about the pattern of the ground motions during a futuristic probable major earthquake if, in case, earthquake occurs in the region under study.

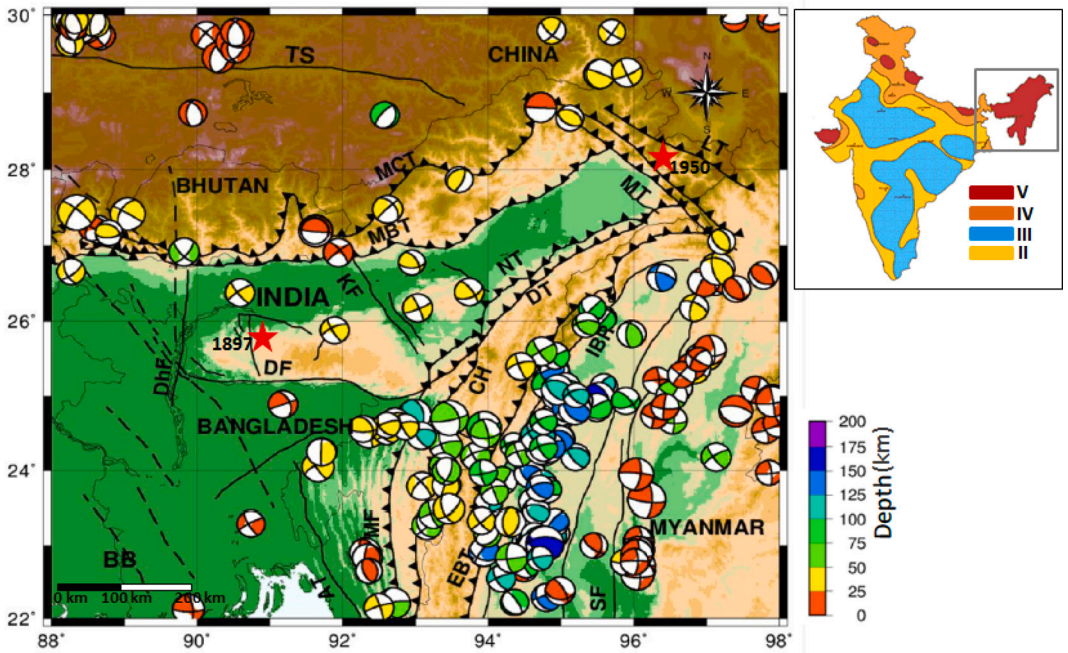

Fig. 1. A map showing the seismotectonic features of the NE India with dispositions of the Main Central Thrust (MCT) and the Main Boundary Thrust (MBT) in north, MishimiThrust (MT) and LohitThrust (LT) in the Eastern syntaxes, Eastern Boundary Thrust (EBT), Indo-Burma Ranges (IBR), and Sagaing Fault (SF) in the Indo-Myanmar region, DhubriFault (DhF),KopiliFault (KF),DaukiFault (DF), Naga Thrust (NT),Disang Thrust (DT),and Chedrang Fault (CH) surrounding the Shillong Plateau,BB represents for Bengal Basin, andArakan Trench (AT). The fault plane solutions of important earthquakes ($7.0 > M \geq 5.5$) since 1976, which are shown in the map depth wise. Inset map shows the Seismic Zonation map of India (BIS, 2002) which divides the country in four zones (different colours) and depicts the entire NE India falls in zone V having the highest seismic hazards.

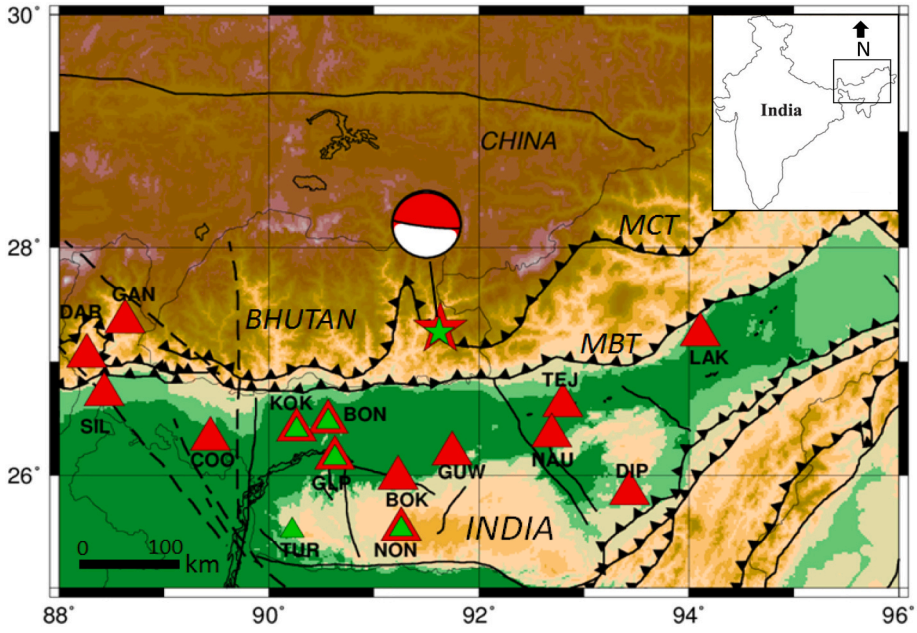

Fig. 2. A map showing the location of the 2009 Bhutan mainshock (M_w 6.1) denoted by the large star and its prominent aftershock (M_w 5.1) [small star] recorded at various stations (large triangles) for the mainshock, and small triangles for the aftershock installed in the NE India. Station codes of the respective stations are shown in the map. Stations KOK, BON, GLP, and NON recorded both the earthquakes (mainshock and aftershock) while TUR recorded only the aftershock event. A fault plane solution of the mainshock is also shown with a beach ball, representing the thrust motion/tectonic regime of the area. Prominent tectonic features (MBT and MCT) are shown in the map, which are same as in Figure1.

2. Seismotectonics of the region

The Indian and the Eurasian plates experience the crustal shortening due to continuous collision in the Himalayan arc region (Tapponnier et al., 1981; 1990; England and Houseman, 1986; Yin and Harrison, 2000; Mishra, 2014; Zhou and Lei, 2016; He et al., 2018) and hence three major well known thrust planes are formed namely Main Central Thrust (MCT), Main Boundary Thrust (MBT) and Main Frontal Thrust (MFT) (Gansser, 1964; Khattri, 1999). As mentioned in the above section, there are mainly four great earthquakes occurred in the Himalaya in past two centuries and since 1950 this region has not met with a great earthquake (Bilham and Gaur, 2000; Khattri, 1999; Seeber and Armbruster, 1981). It is also important to note that the MCT is extremely vivacious tectonic feature of the Himalayan arc and here seismicity is found to be located on a 50-km wide strap between the MCT and the MBT out of which most of the earthquakes are located to the south of the MCT (Khattri et al., 1989; Khattri, 1992; Molnar and Chen, 1982; Seeber and Armbruster, 1981; Valdiya, 1988).

However, the Himalayan region in NE India is one of the most seismically active areas of India and this region has experienced many major and two great earthquakes in the past two centuries which caused tremendous damage to human life and property (Tandon, 1954). The 1897 Shillong earthquake (M 8.1) and 1950 Assam earthquake (M 8.7) are among the great earthquakes according to the published documentations (Oldham, 1899; Tandon, 1954) as also shown in Fig. 1. Although the Himalayan earthquakes are thrust type but various studies have shown as strike-slip mechanisms in Sikkim and Arunachal Pradesh depending upon the local data analysis (De and Kayal, 2003; Kayal, 2008; Kayal et al., 1993; Thingbaijam et al., 2008). The earthquakes are also reported to be with strike-slip mechanisms in the region comprised of eastern syntaxes (Holt et al., 1991). On the other hand, the Indo Myanmar region is also important from a seismic point of view. Many earthquakes have occurred here in past and this region is capable of generating a great earthquake in near future (Gupta and Gahalaut, 2014; Steckler et al., 2016). The earthquakes in the Indo-Mayanmar region occur due to the relative motion of the Indian plate in the eastern direction, whereas based on the GPS studies, it is along the Sagaing and other faults in the region (Gahalaut et al., 2013; Guzman-Speziale and Ni, 1996; Kundu and Gahalaut, 2012; Le Dain et al., 1984; Kumar et al., 2013; Kumar et al., 2015; Steckler et al., 2016). In this region, due to the deep subduction of the Indian plate down to the mantle transition zone, the big mantle wedge has been formed in the Indo-Burma ranges (Mishra, 2011) and is very much corroborative with studies for other regions by other researchers (e.g., Lei et al., 2009, 2019; Lei and Zhao, 2016). As shown in Fig. 1, the majority of earthquakes here occur at a depth range of 30–60 km and the slab steeps in eastward direction causing earthquakes at comparatively deeper depths (Kundu and Gahalaut, 2012; Steckler et al., 2016; Wang et al., 2014; Kumar et al., 2017). Also it is important to note down the Bhutan Himalaya which experienced Bhutan earthquake (M_w 6.1) in 2009 (Kayal et al., 2010) but this region is poorly understood and may have experienced great earthquakes in the last millennium (Diehl et al., 2017; Le Roux-Mallouf et al., 2016) as the decollement present in the western Bhutan region is significantly broader than the central Nepal Himalaya which may lead to produce major to great earthquakes in this region (Le Roux-Mallouf et al., 2015). Various tectonic features of NE India are shown in Fig. 1 along with the fault plane solutions of earthquakes, with $7.0 > M \geq 5.5$, that have occurred in this region from 1976 to 2014 (www.globalcmt.org). We attempted to demonstrate the tectonic setup is very complex and therefore, the role of tectonic configuration and in-situ material heterogeneity of the seismogenic layers in controlling the nature and extent of peak ground acceleration (PGA) in NE India.

3. Strong motion data

The network of strong motion accelerograph (SMA), installed by the Indian Institute of Technology (IIT), Roorkee, sponsored by Ministry of Earth Sciences, New Delhi in the project mode covers the entire Himalayan range from Jammu & Kashmir to NE India. Out of this network few stations are in operation in NE India which are the strong motion accelerographs (SMA) to record the high frequency waves from the earthquakes occurring in this region time to time whereas the accelerographs are also good to record low frequencies of large earthquakes. The instruments of SMA's are of GeoSIG make that has the force-balanced accelerometers and 18-bit digitizers (Mittal et al., 2006; Mittal et al., 2012; Kumar et al., 2012) and are operated in triggered mode at a rate of 200 samples per second (Mittal et al., 2006). There are 30 SMA's installed in different parts of this NE India and most of these are in operation since 2008.

we applied a deterministic approach to the recorded data for analyzing the 2009 Bhutan mainshock (M_w 6.1) and its prominent/strongest and pronoun solitary aftershock (M_w 5.1) have been chosen as

the possible candidates for the simulation of strong ground motion because of vivid source characterization of the events having analogous source distribution (Fig. 2). The mainshock (M_w 6.1) data recorded by a total of 14-stations and the aftershock of this earthquake was recorded at 5-stations as depicted in Fig. 2. The mainshock and aftershock both were recorded by 4-stations and one station has recorded only the aftershock. Table 1 shows the station locations along with the geology of these stations.

4. Methodology

The empirical Green's function (EGF) method is used to simulate the strong ground motions for a target earthquake using actual recordings of small earthquakes as empirical Green's function or as an element earthquake occurred in the same source zone. The advantage of this technique is to use the small earthquake recordings to simulate large earthquakes and small earthquakes contain the path and site effect which also represented in the simulated large event. The target earthquake is generated after inserting the corrections for slip velocity time function of large to small earthquakes. Irikura et al. (1997) gave the modified equations which are depicted below:

$$U(t) = \sum_{i=1}^{N}\sum_{j=1}^{N}\left(r/r_{ij}\right)\cdot F(t)^{*}(C\cdot u(t)) \tag{1}$$

$$F(t) = \delta\left(t - t_{ij}\right) + \left\{\frac{1}{n'^{(1-exp(-1))}}\right\} \times \sum_{k=1}^{(N-1)n'}\left[exp\{-(k-1)/(N-1)n'\}\right.$$
$$\left.\cdot\delta\left\{t - t_{ij} - (k-1)T/(N-1)n'\right\}\right] \tag{2}$$

In eqs. (1) and (2), *U(t)* is synthesized/target earthquake, *u(t)* is element earthquake, *C* is stress drop ratio of target earthquake and element earthquake, *N* is number of grid points for simulation, *T is* rise time of target earthquake, *t* is the rise time of element earthquake, *tij* is the rise time divided by the number of subfaults, *n'* is an integer to eliminate the fake periodicity, *r* is the hypocentral distance from target to the station, *rij* is the distance from the target to the subfault, and * is denoted as the convolution. The element earthquake carries the information of the path and the site, so this method is very useful in simulating the strong ground motions for major/great earthquakes in the various regions (Irikura et al., 1997).

Stress drop ratio between the target and element earthquakes is an important factor due to which PGA values and ground motions are affected. It is also mentioned that the PGA and waveform history also varies with the location of asperity on the fault. These points are also described while calculating the input parameters for simulation in results section. In spite of these limitations, the EGF technique is a powerful technique for estimating strong ground motions at a site where small earthquake recordings are available. The equation to estimate *C* and *N* values are gives as below (Miyake et al., 2003):

$$C = \left(\frac{u0}{U0}\right)^{\frac{1}{2}}\left(\frac{A0}{a0}\right)^{\frac{3}{2}} \tag{3}$$

$$N = \left(\frac{U0}{u0}\right)^{\frac{1}{2}}\left(\frac{a0}{A0}\right)^{\frac{1}{2}} \tag{4}$$

Irikura and Miyake (2011) have explained the method to estimate the source parameters to be used in the simulation. It is hereby noted that the outer fault consists of the entire rupture area comprised of the seismic moment. The inner fault represents the slip within the source, the number of asperities, areas of asperities and stress drop for each asperity. Generally, the seismic activity is found to be lesser within the asperities as compared to the outer regions of the asperities (Irikura et al., 1997; Irikura and Miyake, 2011). Combined area of asperities is computed to be equivalent to 22% of the total fault area for inland earthquakes and 25% for the interplate earthquakes (Somerville et al., 1999). The extra fault parameters are interrelated with the geomorphology of active faults with which the rupture initiation points on the fault can be decided (Irikura and Miyake, 2011). The empirical Green's function method to simulate the strong ground motion has found its vide applicability for different tectonic regions by different researchers (Irikura et al., 1997; Irikura and Miyake, 2011; Miyake et al., 2003; Sharma et al., 2013; Sharma et al., 2016a, 2016b; Sutar et al., 2017; Mittal, 2011), which justifies the use of this methodology to the data used in present study.

5. Results

In the present study, a major hypothetical earthquake (M_w 7.0) has been simulated and the level of ground motions in the NE Indian region is determined. For this purpose, the EGF technique (Irikura et al., 1997) has been used. The recipe of source characterization has been utilized for source scaling to simulate the earthquake scenarios. The 2009 Bhutan Earthquake (M_w 6.1) and its dominant aftershock (M_w 5.1) are used for this study. Earthquake (Mw 5.1) occurred after the occurrence of earthquake of magnitude (Mw 6.1) having the closest location of its mainshock (Mw 6.1) and interestingly the earthquake (Mw 5.1) falls in the same fault plane where the mainshock gets originated, which vindicates the fact that the earthquake (Mw 5.1) was the strongest aftershock of the mainshock (Mw 6.1). A two-step synthesis was formulated; in the first step M_w 6.1 was simulated using data of M_w 5.1 event, and in the second step synthesis M_w 7.0 was simulated using the M_w 6.1 event data. The source parameters for two different earthquakes (M_w 6.1 and

Table 1
Stations used in the present study.

Station name (code)	Station_source	Latitude (°N)	Longitude (°E)	Geology
Darjeeling (DAR)	IITR	27.050	88.262	Gondwana/ Vindhvan
Diphu(DIP)	IITR	25.839	93.435	Pre-Cambrian
Nongstoin (NON)	IITR	25.520	91.260	Pre-Cambrian
Lakhimpur (LAK)	IITR	27.239	94.107	Tertiary
Tura(TUR)	IITR	25.511	90.220	Tertiary
Boko(BOK)	IITR	25.976	91.230	Quaternary
Bongaigaon (BON)	IITR	26.473	90.561	Quaternary
Cooch Vihar (COO)	IITR	26.319	89.440	Quaternary
Gangtok(GAN)	IITR	27.352	88.627	Quaternary
Goalpara(GLP)	IITR	26.152	90.627	Quaternary
Guwahati (GUW)	IITR	26.190	91.746	Quaternary
Kokrajhar (KOK)	IITR	26.400	90.261	Quaternary
Naugaon (NAU)	IITR	26.349	92.693	Quaternary
Siliguri(SIL)	IITR	26.712	88.428	Quaternary
Tejpur(TEJ)	IITR	26.619	92.797	Quaternary

Table 2
Source parameters used for the simulation of Mw 6.1 event using Mw 5.1 data and Mw 7.0 using Mw 6.1 data. M_0 is seismic moment and Vr is rupture velocity.

Element earthquake	First step simulation	Second step simulation
Bhutan Earthquake (aftershock) 29th October 2009 (Mw 5.1) $M_0 = 5.62 \times 10^{16}$ Nm Depth = 5 km (source) Strike = 293°, Dip = 7° and Slip = 107°	Bhutan Earthquake (main shock) 21st September 2009 (Mw 6.1) $M_0 = 1.78 \times 10^{18}$Nm Depth = 8 km Strike = 281°, Dip = 6° and Slip = 94°	Hypothetical Major Earthquake (Mw 7.0) $M_0 = 3.98 \times 10^{19}$Nm Depth = 15 km, 19 km Source1: Strike = 298°, Dip = 6° and Slip = 94° Source2: Strike = 290°, Dip = 10° and Slip = 94°

Vr = 3.0 km/s, Rise time = 0.3 s for Mw 6.1 and 0.9 for Mw 7.0

M_w 7.0) are given in Table 2. The source parameters were estimated on the basis of a recipe to simulate strong ground motion given by Irikura and Miyake (2011) and Miyake et al. (2003).

6. First step simulation

The stress drop ratio (C) and fault dimension (N) are estimated using earthquakes recorded by four stations (KOK, BON, NON and GLP) of the region. One example in Fig. 3(a) and (b) shows the characterized source model obtained to synthesize the earthquake (M_w 6.1) from the event (M_w 5.1). It is observed that simulation of ground motion for estimating reliable PGA values, the size of aftershocks used in the analysis needs to be lesser than two units of magnitude from that of the final simulated earthquake (Irikura et al., 1997). Values a_0, A_0, u_0 and U_0 shown in Fig. 3a have been used to estimate C and N values as per above described method using prescribed eqs. (3) and (4) (Miyake et al., 2003; Irikura and Miyake, 2011). Simulated and observed waveforms for the earthquake (M_w 6.1) are compared for the same stations for the purpose of estimating residual and correlation coefficients through the iterative process. The fault dimensions of length 2.2 km, width 1.8 km, rise time 0.1 s and southern-center point of fault were chosen on the basis of iterations performed until the residual approached zero and correlation approached 1, which achieved only when the observed waveform matches well with the synthetic ones. With the help of estimated values of fault dimensions and the rise time, simulation for all the stations using EW and NS components has been performed as shown in Fig. 3b.

Fig. 4a shows the simulated results for the largest aftershock (M_w 5.1) as the element earthquake and the target observed synthetic for

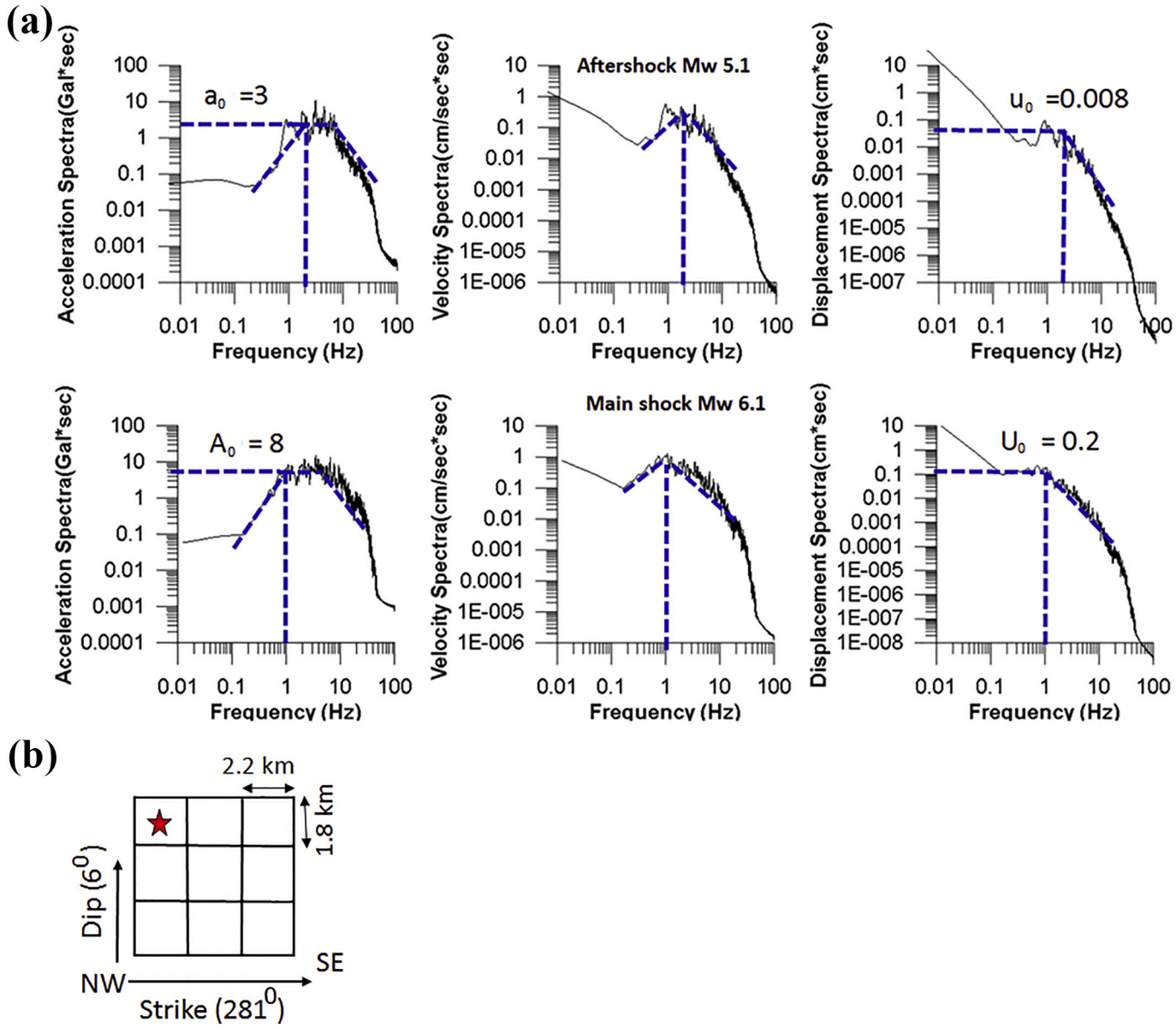

Fig. 3. (a) Plots showing the estimated acceleration, velocity, and displacement spectra, for the mainshock (M_w 6.1) and aftershock data (M_w 5.1) recorded at BON station to validate the EGF method. In acceleration spectra plots, Gal stands for cm/s^2. The values of amplitude of aftershock for given frequency (a_0); A_0 is the same as that of a_0 but for the mainshock from the acceleration spectra, while u_0, and U_0 represent the values of amplitude for the aftershock and the mainshock for the corresponding frequency from the displacement Spectra. Results are based on analysis of different spectra using eqs. (3)–(4) from which C and N values have been estimated. (b) A schematic representation of the characterized source model estimated by source parameterization to synthesize the target earthquake (M_w 6.1) in the first step of synthesis using the element earthquake (M_w 5.1). The parameters of fault dimension are shown as length of 2.2 km and width of 1.8 km for each grid estimated through spectra matching as shown in Fig. 4a, rupture initiation point is shown by a star, strike and dip angles along with the directions are also shown.

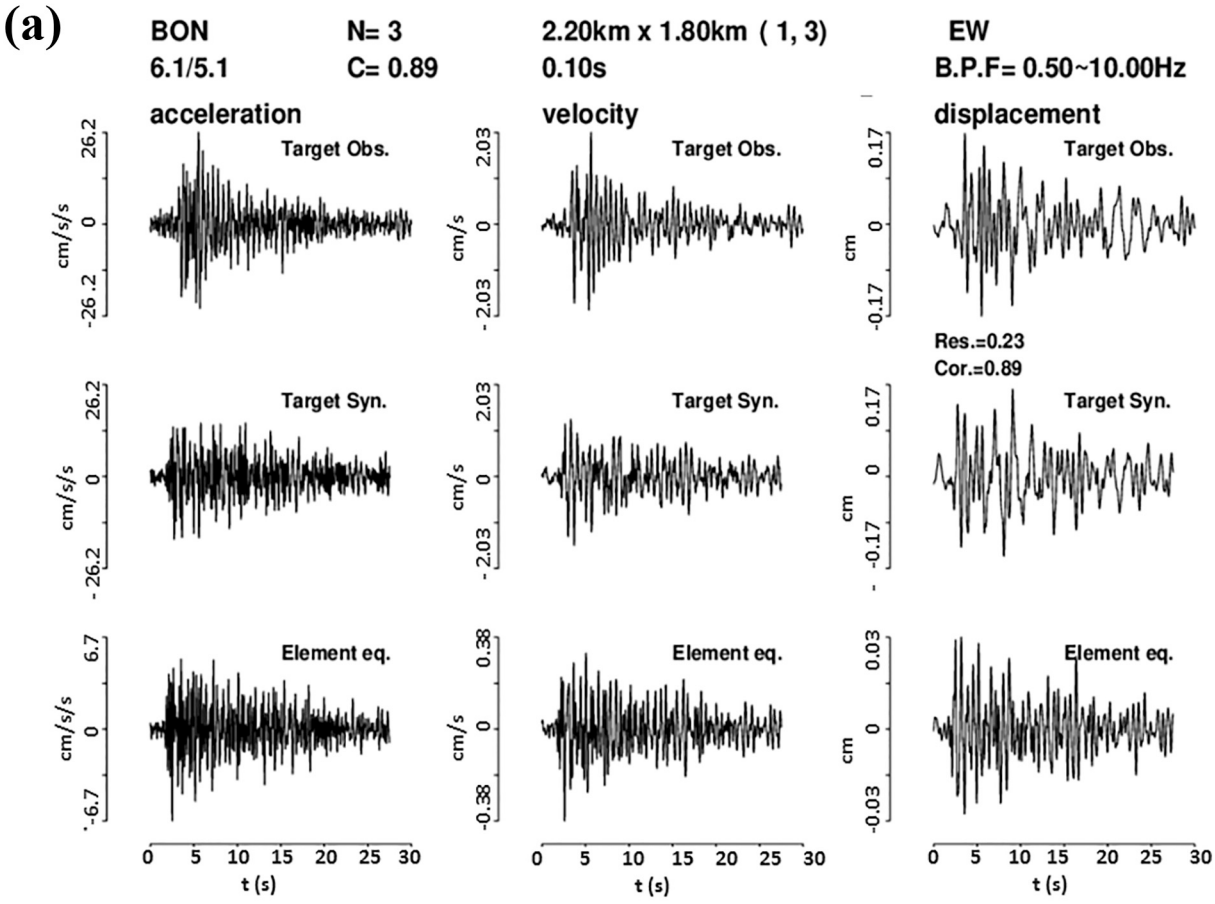
(a)
BON
N= 3
6.1/5.1
C= 0.89
2.20km x 1.80km (1, 3)
0.10s
EW
B.P.F= 0.50~10.00Hz
acceleration
velocity
displacement
Target Obs.
Target Syn.
Element eq.
cm/s/s
cm/s
cm
Res.=0.23
Cor.=0.89
t (s)

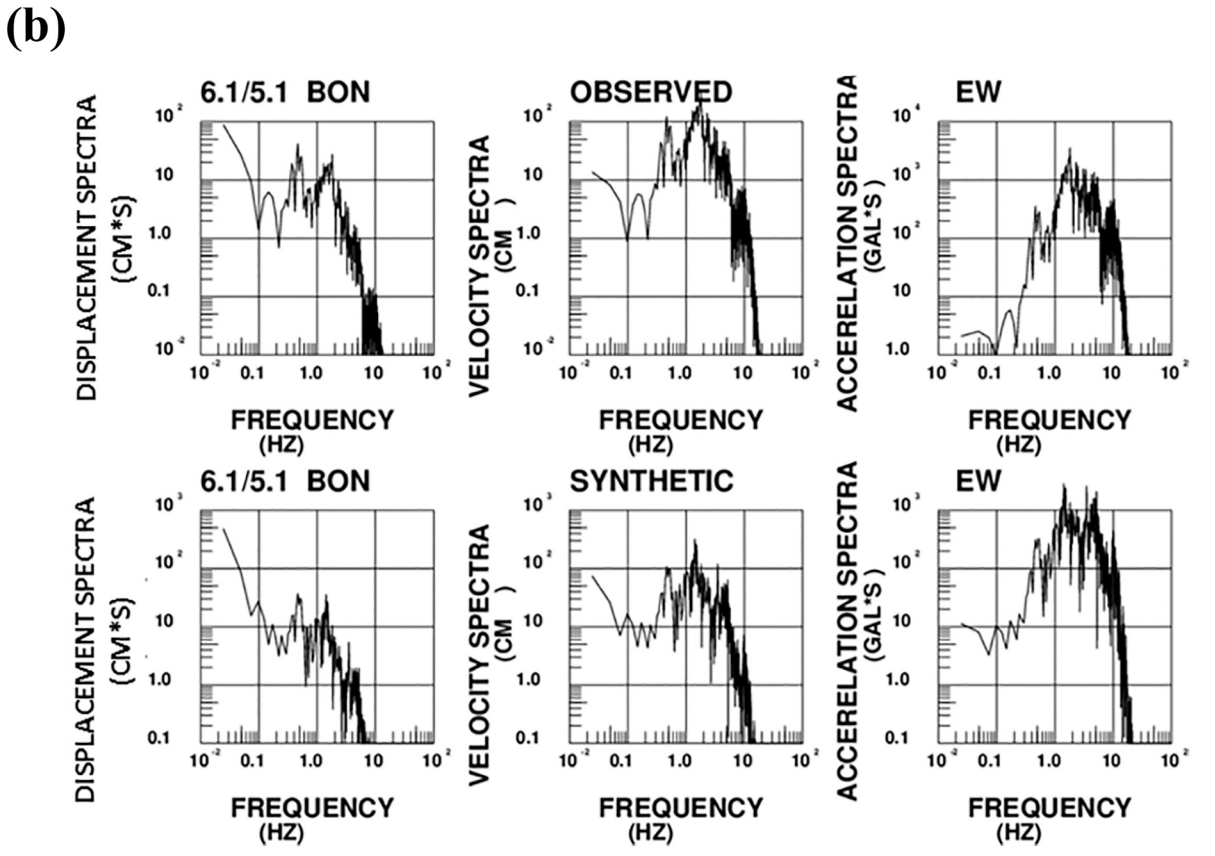
(b)
6.1/5.1 BON
OBSERVED
EW
SYNTHETIC
DISPLACEMENT SPECTRA (CM*S)
VELOCITY SPECTRA (CM)
ACCERELATION SPECTRA (GAL*S)
FREQUENCY (HZ)

Fig. 4. (a) Comparison of Element eq. (earthquake) (M_w 5.1), Target Syn. (synthetic) earthquake (M_w 6.1) and Target Obs. (observed) earthquake (M_w 6.1) waveforms for acceleration, velocity, and displacement recorded and simulated at BON station using data of east-west (EW) component. Band Pass Filter used (B.P.F. = 0.5 to 10 Hz), N, C, dimensions for each sub-fault (length 2.2 km by width 1.8 km) and rise time = 0.1 s are also given. *Res* and *Cor*. correspond to "residual" and "correlation of the observed and synthetic waveforms", respectively. (b) Comparison of the displacement, velocity and acceleration Fourier amplitude spectra for synthetic earthquake (M_w 6.1) and observed earthquake at BON station using the east-west (EW) component data for the first step synthesis. In acceleration spectra plots, Gal stands for cm/s^2. (c) Plots showing the waveforms (upper traces) and Fourier amplitude spectra (lower traces) for acceleration, velocity, displacement for simulated earthquake (M_w6.1) using east-west (EW) component data recorded at TUR station in the first step simulation.

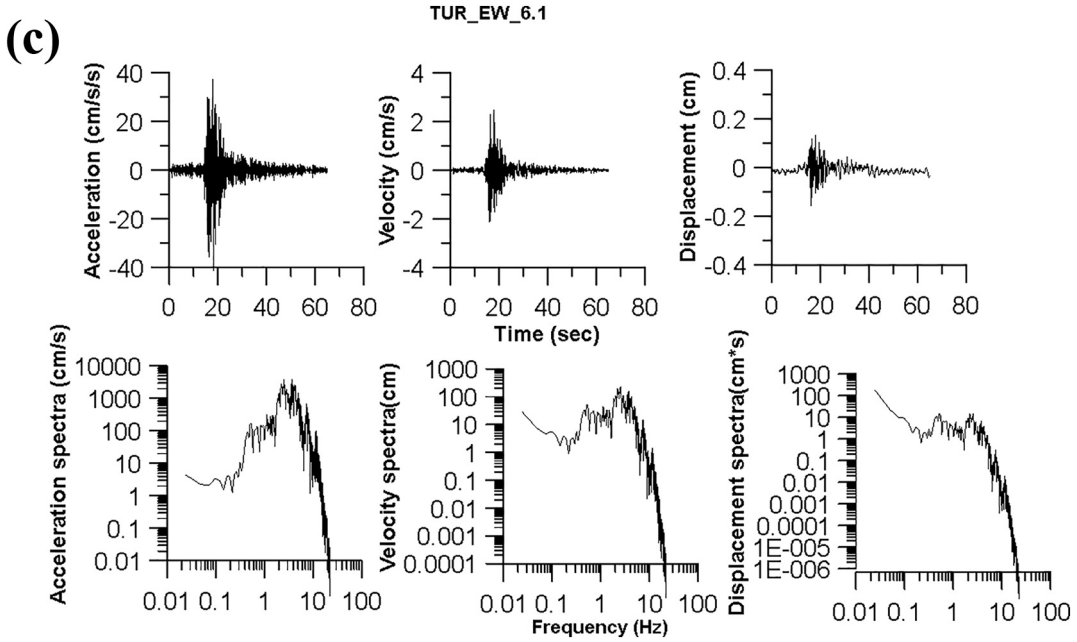

Fig. 4. (*continued*).

acceleration, Velocity and Displacement of the mainshock (M_w 6.1) recorded at station BON. Fig. 4b shows the Fourier spectra of synthetic and observed waveforms for BON station and it is seen that Fourier spectra of observed and synthesized waveforms are comparable to each other. After getting these results for all the stations for EW and NS components, the waveforms for the earthquake (M_w 6.1) using TUR station are synthesized using the same source parameters as shown in Fig. 4c, as this station did not record the mainshock (M_w 6.1). The results for station TUR simulated earthquake and spectra for acceleration, velocity and displacement are shown in Fig. 4c. The EGF technique is validated matching observed spectra with that of the simulated spectra for the earthquake (M_w 6.1) data for stations BON, KOK, GLP and NON.

7. Second step simulation

After validating the EGF technique for NE India, a hypothetical earthquake was simulated using waveforms of mainshock (M_w 6.1) data for fifteen stations in the target area. The source parameterization of the first step simulation was extended to make it a source for the earthquake (M_w 7.0) for the second step simulation using the formulations given by Somerville et al. (1999), Miyake et al. (2003) and Irikura and Miyake (2011). In first step of simulation stress drop (C) and fault dimension (N) are estimated to simulate M 6.1 while in the second step to simulate M 7, the first step fault is being taken as one grid point and other parameters are estimated by empirical relations (Somerville et al., 1999; Miyake et al., 2003; Irikura and Miyake, 2011) in the second step keeping the stress drop ratio same for second step as that of the first step. In accordance to seismotectonics and available fault plane solutions as shown in Fig. 5a of the region, a fault has been positioned for two cases (targets 1 and 2). The red rectangle within the fault is the asperity for a major earthquake (M_w 7.0), which can be considered the strong motion generation area (SMGA). The two small red stars in Fig. 5a are the scenarios N1 and N2 for target 1 and S1 and S2 for target 2 cases. The geometry of the fault is shown in Fig. 5b and radial propagation of the wave is considered for the present study. Table 3 shows the fault parameters used for the simulation of the earthquake (M_w 7.0) extrapolated from the earthquake (M_w 6.1) data as discussed above. Fig. 6a shows the relation of SMGA with respect to magnitude and seismic moment in order to validate the input parameters used in the present study (Miyake et al., 2003). Similarly, Fig. 6b is for the relation of rise time with respect to moment magnitude and seismic moment. The estimations for the SMGA and rise time for the present study cases for earthquakes of varying strengths (e.g. M_w 5.1, 6.1, and 7.0) are comparable to the scaling relations as shown in Fig. 6a and b.

Fig. 7a shows the simulated waveforms and spectra for station BON for the case of the hypothetical major earthquake (M_w 7.0). The frequency band used to simulate this earthquake is taken as 0.2 to 10 Hz. Fig. 7b shows the acceleration, velocity and displacement for SMGA, background area, and characterized source model (combined values for SMGA and background area) using the earthquake (M_w 6.1) recorded at BON (EW component) along with the peak values of PGA written with the waveform. Fig. 7c shows the simulated acceleration for two scenarios N1 and N2 using EW (1st and 2nd column) and NS (3rd and 4th column) components for 14-stations using earthquake (M_w 6.1) as an element earthquake and Fig. 7d shows the waveforms for S1 and S2 using EW (1st and 2nd column) and NS (3rd and 4th column). Table 4 shows the PGA values computed for 14-stations, for target 1 (N1 and N2 scenarios) and target 2 (S1 and S2 scenarios) using EW and NS components, with respect to epicentral distance from each station. Here, it is interesting to note that PGA values at respective sites are corroborated with respective geology of the sites as shown in Table 1 such as GLP shows the highest PGA being situated on the Quaternary formations as compared to DAR having Pre-cambrian geology exposed. Fig. 8 shows the comparison of calculated PGA values for N1, N2, S1 and S2 scenarios using EW and NS components with the ground motion prediction equation developed by Sharma et al. (2009) for earthquake (M_w 7.0),

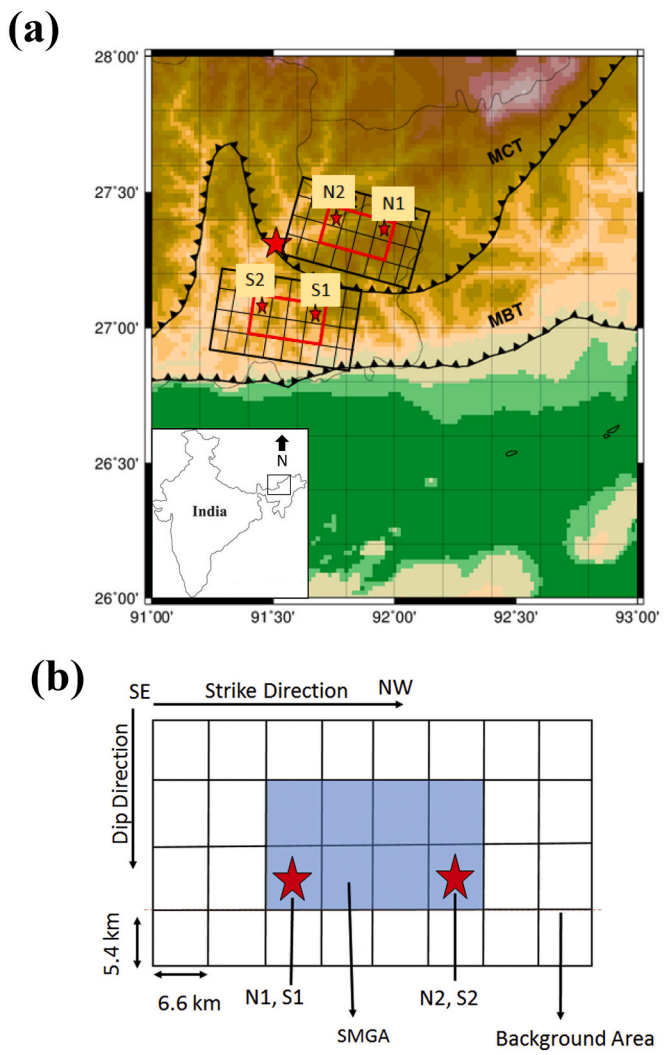

Fig. 5. (a) Schematic representation of two targets (faults) positioned in the Bhutan Himalayan region. The MCT and the MBT are the same as in Fig. 1. Small rectangles on the fault planes show the Strong Motion Generation Areas (SMGAs) and rest areas are depicted as the background areas. Two small stars are scenarios (rupture initiation points) N1 & N2 (above) and S1 & S2 (below). A large star represents the epicentre of the 2009 Bhutan mainshock (M_w 6.1). The dip and strike directions of the fault are also conformable to the geology and seismotectonics of the region. (b) A schematic diagram showing the fault geometry (length 6.6 km and width 5.4 km for each grid) to simulate earthquake (M_w 7.0) in the second step simulation along with the Strong Motion Generation Area (SMGA) depicted with shaded region, background area shown in white colour and scenarios (N1 & N2)/(S1 & S2) for target 1 and target 2 respectively are depicted by two stars. The strike and dip values considered in the two cases have been provided in the Table 2.

Table 3
Source parameters used for simulating the earthquake (Mw 7.0) using the Mw 6.1 data in the north-east India (SMGA corresponds to strong motion generation area).

Parameter	SMGA	Background area
Rupture area	285 km^2 (Somerville et al., 1999)	1113 km^2(Somerville et al., 1999)
No. of sub-faults	4 × 2 (Miyake et al., 2003)	8 × 4 (Miyake et al., 2003)
Strike, Dip, Rake	Strike = 298°, Dip = 6° and Slip = 94° for Target 1 and Strike = 290°, Dip = 10° and Slip = 94° for Target 2	Strike = 298°, Dip = 6° and Slip = 94° for Target 1 and Strike = 290°, Dip = 10° and Slip = 94° for Target 2

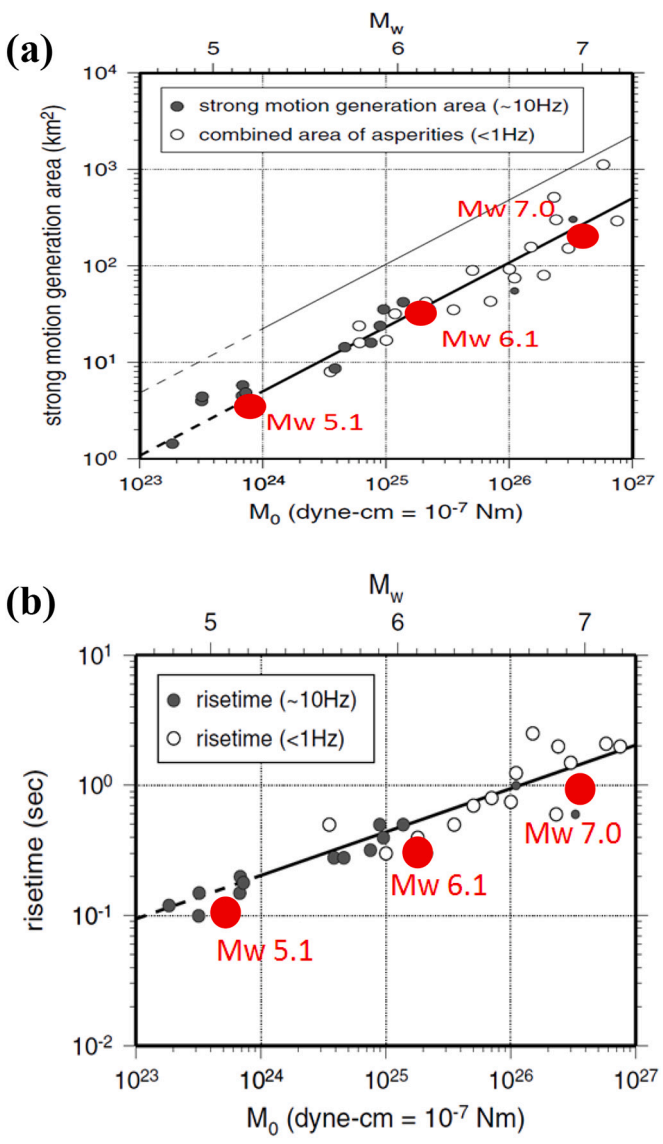

Fig. 6. (a) A graph representing the scaling of strong motion generation area (SMGA) with magnitude and seismic moment where thick and thin lines are for the combined areas of asperities and total rupture area. Solid and open circles show strong motion generation area and combined area of asperities by Somerville et al. (1999). Three large dots show the comparison of the estimated SMGA for the present study (modified after Miyake et al., 2003). (b) A plot showing the scaling of rise time with magnitude and seismic moment where thick line shows the scaling of rise time by Somerville et al. (1999). Three large dots show the comparison of estimated rise time for the present study (modified after Miyake et al., 2003).

which is valid for the Himalayan region. In this study the estimated PGA falls in the range of 8 cm/s^2 to 121 cm/s^2 for distances between 361 and 126 kms respectively (Table 4). The PGA at station GLP, at a distance of 160 kms, is the highest of all the stations. The lowest PGA is at station GAN which lies nearly 319 kms away from the epicentre. The results show the effect of rupture directivity and site amplification of the ground motions in the area. In the case of the 2009 Bhutan earthquake (M_w 6.1) considerable damage to buildings was reported at stations GUW and GLP. The PGA of simulated earthquke (M_w 7.0) shows that the damage in the vicinity of stations GUW, GLP and BON would also be very likely, as these stations show a PGA in range from 80 to 113 cm/s^2 (Table 4). The simulated waveforms show that the maximum duration of the waveform for estimated PGA that corresponds to the south and south-west part of the study region (Fig. 7c and d).

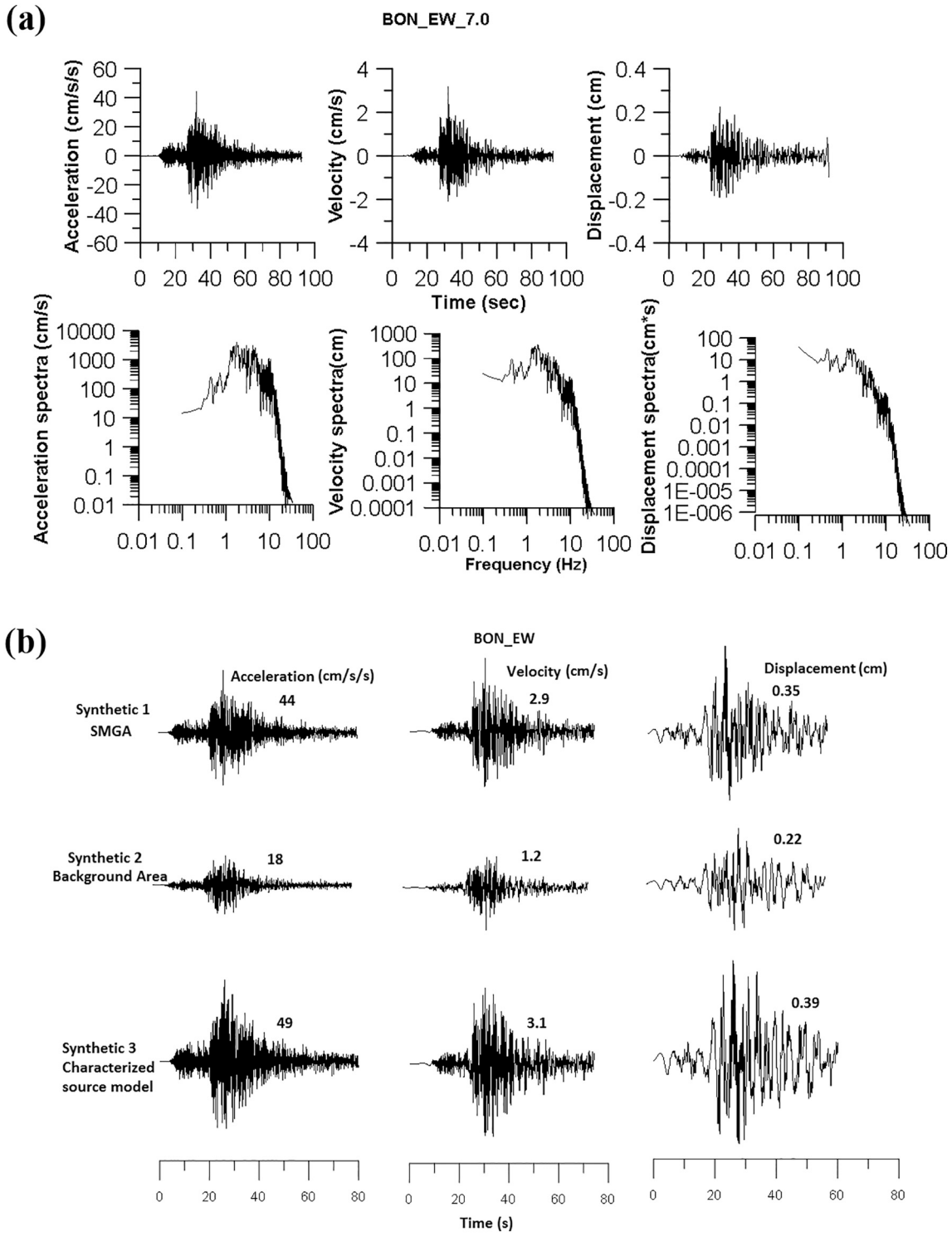

Fig. 7. (a) Plots showing the simulated waveforms (upper traces) and Fourier amplitude spectra (lower traces) for TUR station (acceleration, velocity, and displacement) for the synthetic earthquake (M_w 7.0) using the 2009 Bhutan mainshock (M_w 6.1) as an element earthquake (EW component) in the second step simulation using band pass filter for the range of 0.2 to 10 Hz. (b) Plots showing the acceleration, velocity, and displacement for SMGA (above-Synthetic 1), background area (middle-Synthetic 2), and characterized source model (lower-Synthetic 3) for simulated synthetic earthquake (M_w 7.0) using the mainshock (M_w 6.1) recorded at BON (EW component) in the second step simulation. The corresponding peak values for all the results have been written for each plot. (c) The simulated earthquake (M_w 7.0) acceleration for target 1, scenarios N1 and N2 using EW components (1st& 2nd column) and NS components (3rd & 4th column) respectively for fourteen stations using Bhutan mainshock (M_w 6.1) as an element earthquake for the second step simulation. Stations differentiated for different direction of rupture as SW, SE and S based on the location of stations from source. (d) The simulated earthquake (M_w 7.0) acceleration for target 1, scenarios S1 and S2 using EW components (1st& 2nd column) and NS components (3rd& 4th column) respectively for fourteen stations using Bhutan mainshock (M_w 6.1) as an element earthquake for the second step simulation. Stations differentiated for different direction of rupture as SW, SE and S based on the location of stations from source.

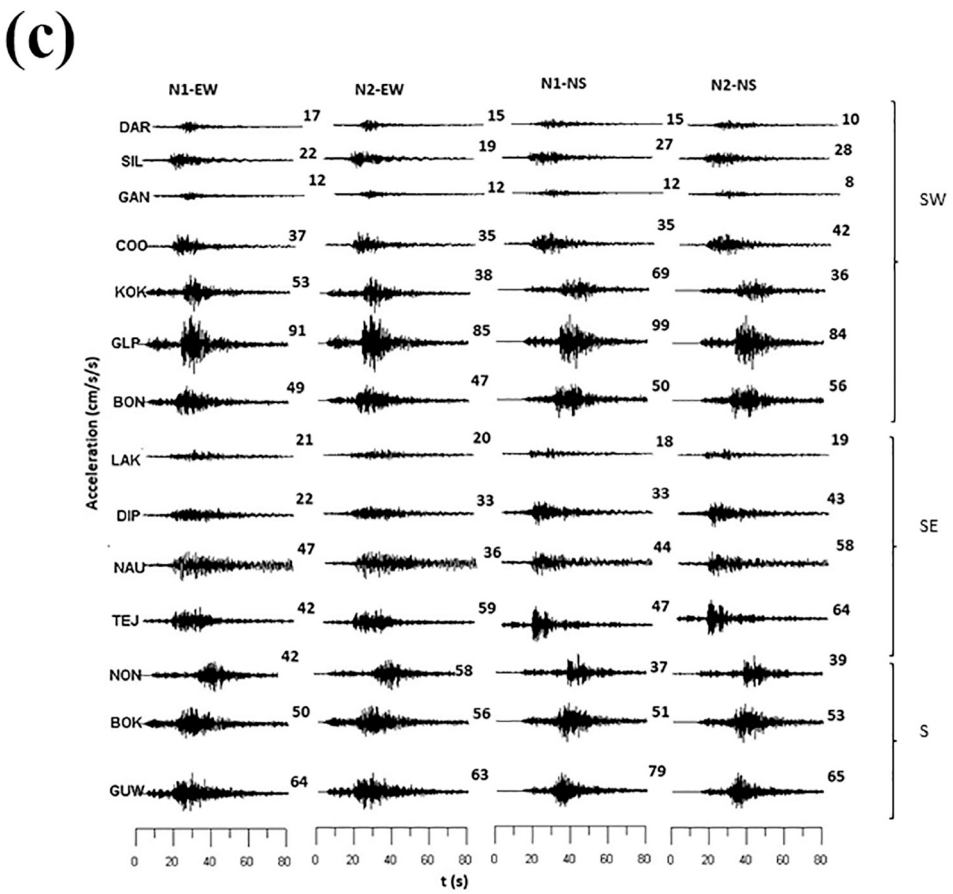

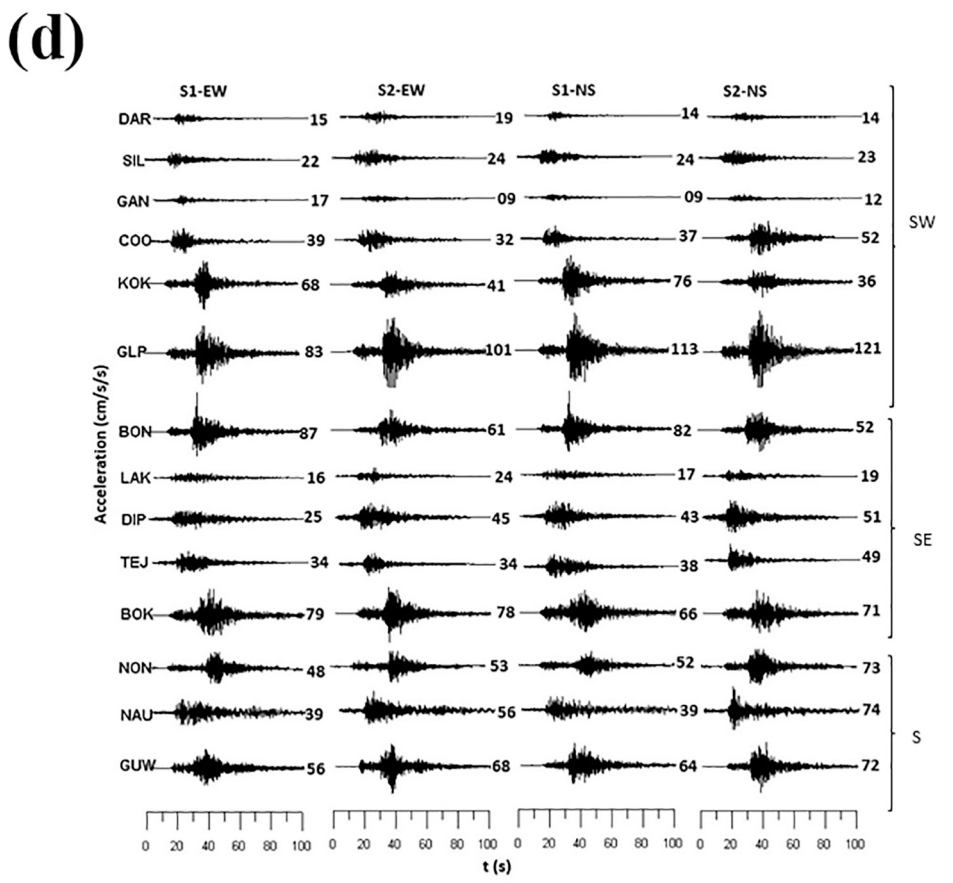

Fig. 7. (*continued*).

Table 4
Peak ground accelations (PGAs) computed for 14 stations (station code), for simulation (N1 and N2 scenarios) and for simulation (S1 and S2 scenarios) using EW and NS components.

Station code	N1_EW (cm/s/s)	N2_EW (cm/s/s)	N1_NS (cm/s/s)	N2_NS (cm/s/s)	S1_EW (cm/s/s)	S2_EW (cm/s/s)	S1_NS (cm/s/s)	S2_NS (cm/s/s)
BOK	50	56	51	53	79	78	66	71
BON	49	47	50	56	87	61	82	52
COO	37	35	35	42	39	32	37	52
DAR	17	15	15	10	15	19	14	14
DIP	22	33	33	43	25	45	43	51
GAN	12	12	12	8	17	9	9	12
GLP	91	85	99	84	83	101	113	121
GUW	64	63	79	65	56	68	64	72
KOK	53	38	69	36	68	41	76	36
LAK	21	20	18	19	16	24	17	19
NAU	47	36	44	58	39	56	39	74
NON	42	58	37	68	48	53	52	73
SIL	22	19	27	28	22	24	24	23
TEJ	42	59	47	64	34	34	38	49

The comparisons of simulated PGA values with GMPE by Sharma et al. (2009) shows PGA tended to decrease with respect to distance (Fig. 8). The dark line is for the validity of the GMPE up to 200 km and after that PGA is extended based on the same relation, which is shown by dashed line after solid line. On the other hand, it is important to note that at lesser distances, few PGA values are overestimated than GMPE and at greater distances also few PGA values are smaller than the GMPE. This may be due to the effect of rupture directivity and site amplification of ground motions which are not included in GMPE for lesser distances. The GMPE is valid up to 200 km of fault distance, therefore futher investigation of ground motion attenuation is needed for greater distances by introducing more data. Fig. 9 shows the comparison of rupture directivity for the simulated PGA in the study area with different rupture initiation points (N1, N2, S1, S2) using EW (a,c,e,g) and NS (b,d,f,h) componets of the simulated waveforms. Here it is interesting to note that the S1 and S2 are the worst among the four chosen scenarios, whereas the rupture is found propagated towards south-west from the source locations, hence the stations located in south west to the source (e.g., BOK, GUW, NON and GLP) show maximum PGA values. We simulated a schematic model as shown in Fig. 10 that demonstrates how the formational geology beneath different seismographic recording stations control the nature and extent of variability in PGA values for better understanding of factors that cause the seismic amplifications of subsrface materials, which may have strong bearing to seismic hzards to the structures located in the areas of influence.

8. Discussion

The present study is an attempt to assess the NE Indian region deterministically to estimate the PGA and waveform histories at various sites. NE India is the part of Himalayan arc which is the region of great concern in this regard as it is tectonically complex and hence seismically very active. So far, the Probabilistic Seismic Hazard Assessment (PSHA) has been performed in several previous studies for different parts of India including NE India (Khattri et al., 1984; Bhatia et al., 1999; De and Kayal, 2004; Nath et al., 2008; Sitharam et al., 2015). For NW India Khattri et al. (1984) suggested that this region can expect PGA range of 0.4 g (392 cm/s/s) to 0.7 g (686 cm/s/s) with a 10% probability of exceedance in the next 50 years. Similarly, Bhatia et al. (1999) estimated PGA between 0.1 g (98 cm/s/s) and 0.3 g (294 cm/s/s) with a 10% probability of exceedance in next 50 years for the Himalayan region. The variation in the results depends on the region of study and data used in the analysis. On the other hand, Parvez et al., 2003 estimated a Deterministic Seismic Hazard Assessment of India and for NE India, the acceleration output is in between 0.3 (294 cm/s/s) to 0.6 g (588 cm/s/s). However, it has been found that the NW Himalayan region is liable to expect PGA between 0.02 g and 0.5 g with a 10% probability in 50 years (Mahajan et al., 2010). Correspondingly, Shaligram et al. (2014) estimated high hazard for a 2% probability of exceedance in 50 years for Himalayan region whilst Sriram and Khattri (1999) calculated PGA for Kangra region using composite source model which gave PGA of 0.7 g (686 cm/s/s). Likewise, Dinesh et al. (1999) gave hazard assessment for the NW Indian region. Similarly, the study of microzonation and seismic hazard assessment for NE India have been taken up by Nath et al., 2008 and showed a high seismic hazard in the Brahmaputra valley and Sikkim regions. Most recently, it has been observed that the 2015 Nepal earthquake (M_w 7.9) had great impact in the border areas of India to Nepal especially at Motihari district where PGA was recorded maximum among the stations at Indian side at a distance of 166 kms (Sharma et al., 2017). PGA distribution for this earthquake showed the distinct partitioning of the PGA values in the area of Indo-Gangetic plains depending on the rupture directivity, geological constraints and site effects (Sharma et al., 2017). The cities lying in the Indo-Gangetic plane area were affected by considerable loss of human life and property by the 2015 Nepal earthquake (Sharma et al., 2017). Henceforth the entire Himalayan arc has the potential to generate a great earthquake in near future and consequently the NE India also comes under this threat (Gupta and Gahalaut, 2014). Seismological constrictions related to major earthquakes occurred in Himalaya are subjected to urgent requirement for earthquake hazard assessment and disaster mitigation in the Himalayan region (Srivastava et al., 2010) where the influence of surface waves on tall structures and longer duration of shaking need to be ascertained (Mishra, 2014; Nath and Thingbaijam, 2012; Nath et al., 2008).

Keeping in view, the several studies available related to the present study, an attempt has been made to estimate ground motions for a major earthquake for the NE Indian region. The source of the earthquake is kept in the Bhutan Himalaya same as that of 2009 earthquake because this region is poorly understood, but it may have experienced great earthquakes in the past era (Roux-Mallouf et al., 2016; Diehl et al., 2017). The presence of the complex tectonic regime herein is the important factor to consider this region as a great concern towards the seismic hazard assessment (Mishra, 2014). The level of ground accelerations expected in this region for a hypothetical major earthquake (M_w 7.0) has been ascertained. As an outcome the estimated PGA is in the range of 8 to 121 cm/s/s for distances between 361 and 126 kms respectively. The border areas of India to Bhutan are also vulnerable to earthquake risk that may have potential for expected high level of damage to structures during strong ground motions. The present analysis demonstrated that PGA-variation from 8 cm/s/s to 121 cm/s/s for distances between 361 km and 126 km has bearing on the future construction in the area that can be regulated and maintained accordingly to reduce the risk of future probable earthquake (M_w 7.0) in the region of study, when PGA reflects combined effects of tectonic and in-situ site characteristics of seismogenic layers. The expected acceleration in the Brahamputra valley with the excedance of 100 cm/s/s is quiet high as

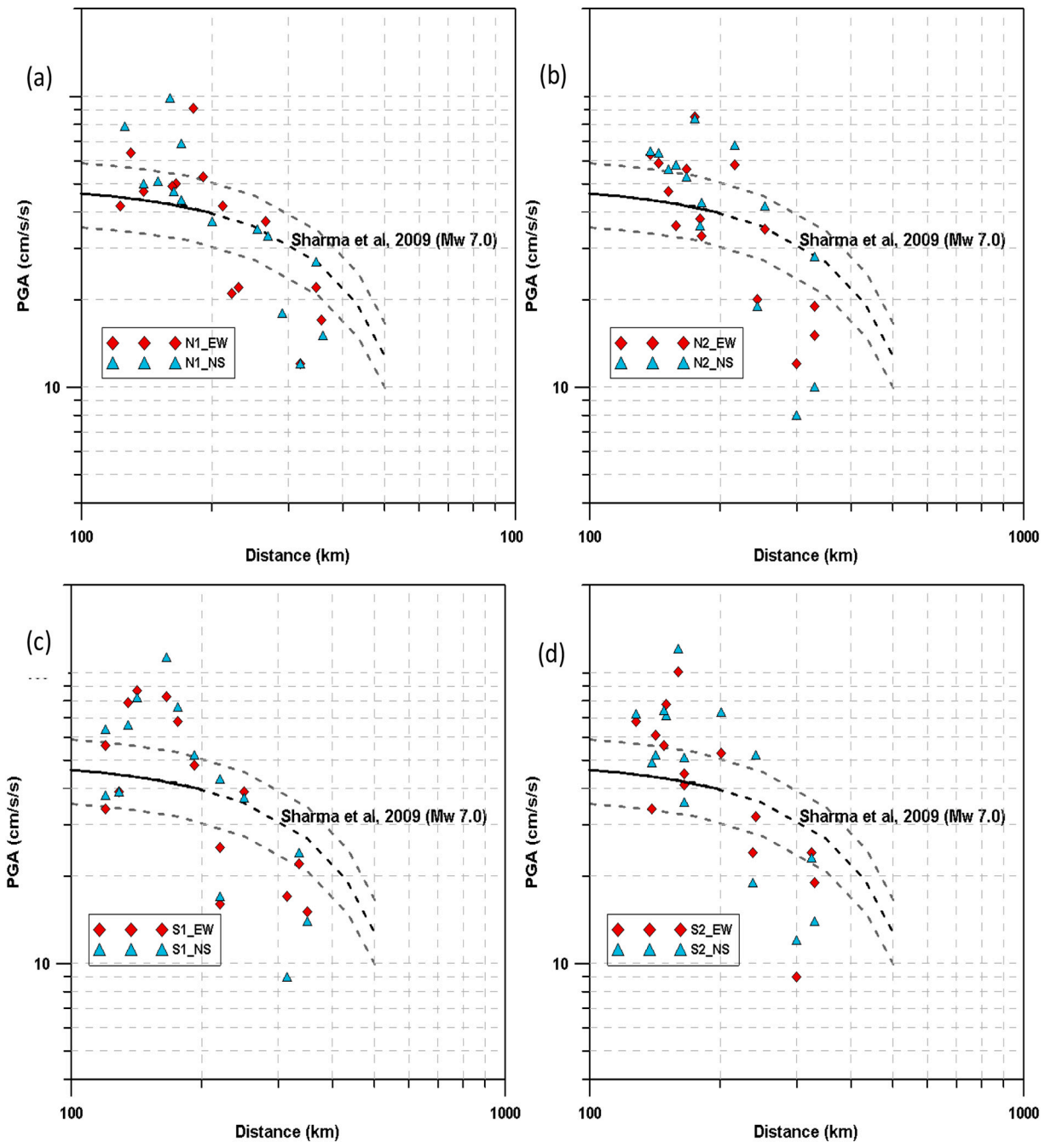

Fig. 8. Comparison of calculated PGA values for different rupture initiation points N1 (a), N2 (b), S1(c), S2(d) using EW & NS components with ground motion prediction equation devloped by Sharma et al. (2009) shown with black dashed line for simulated earthquake (M_w 7.0) in second step simulation. Above & below grey dashed lines represent ±1 standard deviation.

this region is comprised of quaternary sedimants of young ages. This affects the ground motion to be amplified because the ground motions are trapped in the sediments and require more time to pass through, hence have the bigger amplitudes. In case of major to great earthquakes this situation may be more severe because of the resonance effect imposed.

On the other hand, the different rupture initiation points utilized (Fig. 5a) in the present study gives the important requirement of the construction design practices. GLP site exhibits the maximum PGA in all the scenarios while BON shows 82 cm/s/s for S1 scenario (NS component) and 87 cm/s/s for S1 scenario (EW component) as shown in Table 4. It is important to note the changes in the PGA at various sites when the initiation point is changed. It is worth to be noted that the simulated waveforms show the maximum duration of the waveforms and PGA in the south and south-west part of the study region (Fig. 7c and d), which suggests that the simulated ground motion is dictated by the PGA and wavefrom histories, reflecting combined effects of local tectonic and in-situ site characteristics of the seismogenic layers that can be treated as a well constrained condition for regulating the earthquake risk mitigation plans as the future strategy to deal trans-boundary disastrous earthquakes for NE-India (Fig. 7a–d).

When we compare the simulated PGA values with the existing GMPE (Fig. 8), it is seen that the the PGA gets decrease with respect to distance but at small and larger distances the PGA values are not comparable because of the dependncy of the actual ground motions decay with the source, path and site characteristics (Dujardin et al., 2016; Sandhu et al.,

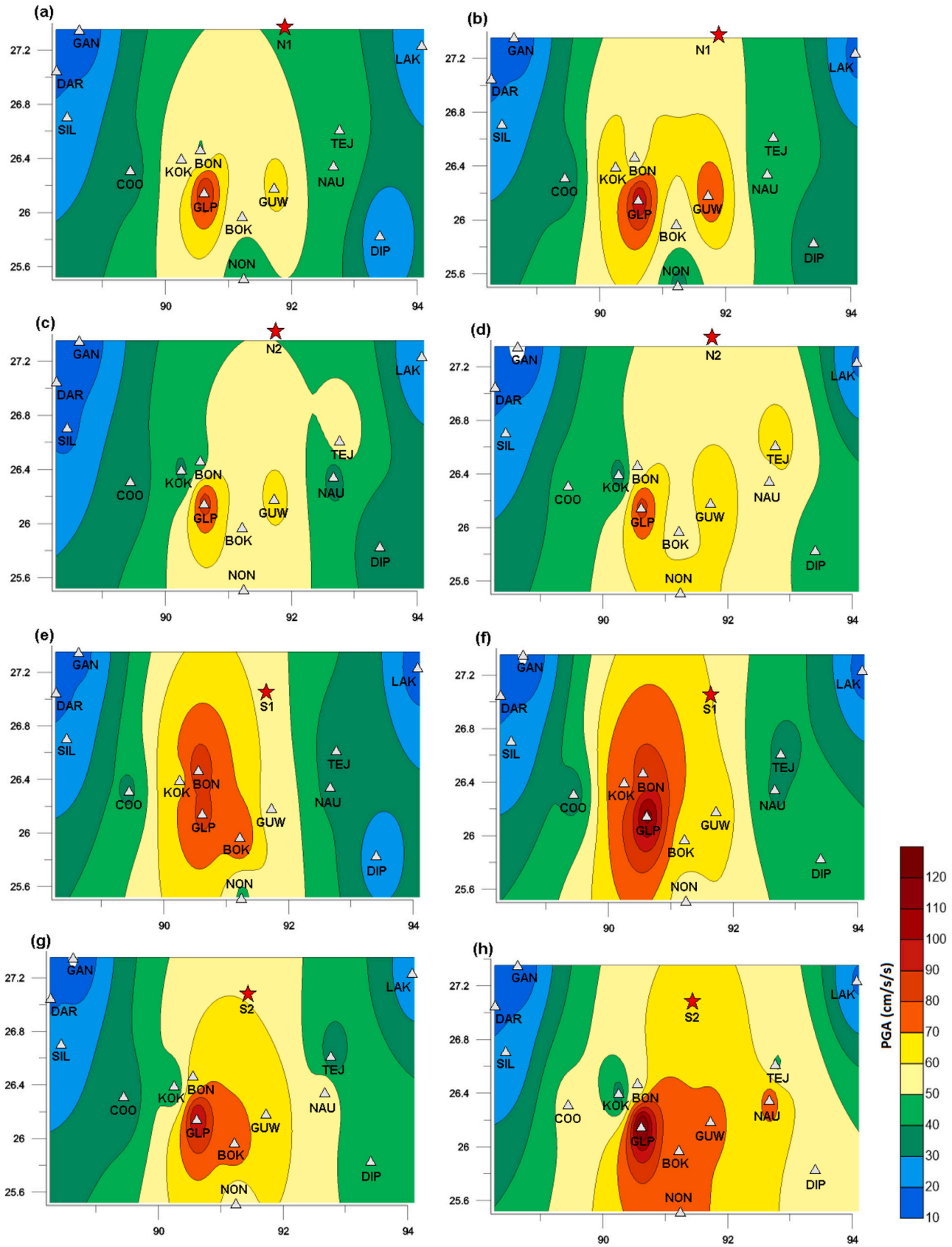

Fig. 9. Comparison of Rupture directivity for the simulated PGA in the study area with different rupture initiation points (N1, N2, S1, S2) using EW (a,c,e,g) and NS (b,d,f,h) componets of the simulated waveforms.

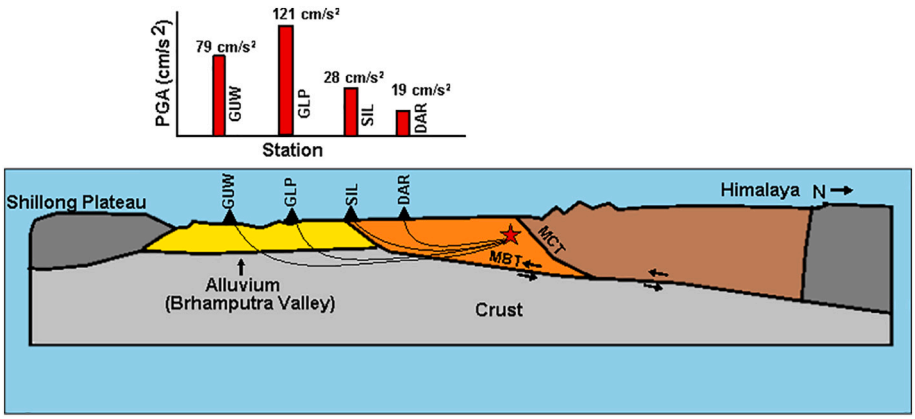

Fig. 10. A schematic demonstration of the results for four stations in terms of a model that depicts wave paths in different geological formations along with the corresponding PGA values obtained in the simulation. DAR and SIL stations are located SW to the source, however GLP and GUW correspond to the south with respect to the source as shown in Fig. 2. The anatomy of the underneath Himalaya is taken from previous studies (Seeber and Armbruster, 1981; Valdiya, 1988), which is corroborative with similar studies for other parts of the Himalaya (Kayal et al., 2010; Mishra, 2014; He et al., 2018).

2020) and all these effects are not introduced in the GMPE's. There is discrepancy between the decreasing of GMPEs with distance, it is also interesting to consider that the PGA decrease with distance is different for large and small earthquakes given their different frequency content resulting in different effect of attenuation on them as shown in Fig. 8. Also, S1 and S2 are observed to be the worst cases among the four chosen scenarios. In order to validate our ground motion simulation, we also attempted to see the nature and extent of rupture directivity of the expected earthquake (Mw 7.0) with respect to four rupture initiation points (Fig. 9). It is found that impacts of higher values of PGA and the shaking duration correspond to either South or South-West direction of the expected source locations, which in turn suggests that areas of maximum ground shaking would be observed for settlements in the vicinity of the source locations, causing expectedly more earthquake hazards in the NE-Indian region. It is evident from the disposition of rupture directivity of the simulated earthquake (Mw 7.0) that the rupture propagates towards the south-west of the source location, hence the stations locating in the south west to the source (e.g., BOK, GUW, NON; GLP) are associated with the maximum PGA values (Fig. 9). Our schematic model as shown in Fig. 10 also validates and demonstrates that material heterogeneities associated with weaker alluvial materials have strong bearing towards enhancement of PGA values with reference to stations GUW and GLP whilist the comparatively stronger geological formations beneath the stations SIL and DAR corresponds to the lesser values of PGA, which depicts wave paths in different geological formations along with the corresponding PGA values obtained in the simulation. This observation is found to be in good unison with attenuative behaviour of the soft geological formations related to shallow sediments of different categories (Mishra et al., 2020a).

NE India is very important with respect to its unique geotectonic locations and for the development of infrastructural facilities related to multi-purpose hydro-electric power and nuclear power plants, dams, bridges, and vital installations where prevalence of poor construction practices are still found to be very imminent. In order to develop the risk resilient constructions as under its future the construction engineers need this kind of inputs in designing important buildings such as dams, bridges, nuclear power plants. It is so because the source locations have strong influences on the changes in PGA values with change of initiation points. This study provides one step forward towards enrichment of our understanding for making assessments of seismic hazards in the target area that may also be applied to areas having similar tectonics for development of the corresponding model for earthquake risk resilient through site characterization of the seismic zones based on seismic microzonation study (Mishra, 2012; Mishra, 2020; Mishra et al., 2020b). The results of this piece of study are helpful to assess seismic hazards in the target area, which can be useful for the engineering community.

9. Conclusions

In the present study, the EGF approach has been utilized to model a major earthquake (M_w 7.0) using observed ground motions for the Bhutan earthquake (M_w 6.1) and its largest aftershock (M_w 5.1) which occurred in close proximity of the Bhutan Himalaya. The level of ground motions for the earthquake (M_w 7.0) is compared with ground motion prediction equation for the Himalayan region. This study is the first of its kind to estimate PGAs as well as ground motion time histories using the actual recordings of the small earthquake in NE India. It has been observed that PGA values are found to be comparable to the ground motion prediction equation with respect to fault distance. The present study using the EGF technique has provided constraints on the level of accelerations experienced during a scenario earthquake (M_w 7.0) and its impact in NE India. It has been observed that the towns near to the rupture initiation may experience large ground accelerations during the shaking generated by the earthquake (M_w 7.0) and many stations in the study region may expect acceleration in excess of 100 cm/s^2. The present analysis demonstrated that PGA-variation from 8 cm/s^2 to 121 cm/s^2 for distances between 361 km and 126 km has bearing on the future construction in the area that can be regulated and maintained accordingly to reduce the risk of future probable earthquake (M_w 7.0) in the region of study, when PGA reflects combined effects of tectonic and in-situ site characteristics of seismogenic layers. Our results clearly demonstrate that material heterogeneities associated with weaker alluvial materials have strong bearing to enhancement of PGA values whilist the comparatively stronger geological formations corresponds to the lesser values of PGA, which depicts wave paths in different geological formations along with the corresponding PGA values obtained in the simulation. This study is important in socio-economic point of view because ground motions estimated here are helpful for the engineering community for planning future construction and retrofitting existing structures in the region. Therefore, it is concluded that the present study may be useful for assessing seismic hazards in the target area, which can also be applied to areas of similar kinds of tectonics to develop a model for earthquake risk resilient through site characterization of the seismic zones by Seismic Microzonation.

Data and resources

Maps in the manuscript are prepared using the Generic Mapping Tool (GMT). The fault plane solutions are taken from www.globalcmt.org/CMTsearch.html (last accessed August 2017). The network of strong motion accelerograph (SMA), installed by the Indian Institute of Technology (IIT), Roorkee, sponsored by Ministry of Earth Sciences, New Delhi in the project mode covers the entire Himalayan range from Jammu and Kashmir to NE India. Out of this network few stations are strong motion accelerographs (SMA) in operation for the NE India which

record high frequency waves from the earthquakes occurring in this region time to time. The data of this network has been used in the present study.

Authors declaration

Authors declare that there is no competing interest in publishing this research article. It is further stated that the entire work is based on analysis of data at NCS-MoES, India without any financial sponsorship from any agency.

Declaration of Competing Interest

Authors have no conflict of interest with any component of this piece of research and study, which has been carried out independently using their own data set with available research facilities of National Centre for Seismology, Ministry of Earth Sciences for the benefit of science and society.

Acknowledgements

BS and OPM are thankful to Prof. Shailesh Nayak, Former Secretary and Dr. M. Rajeevan, present Secretary, Ministry of Earth Sciences for their consistent motivation since the commencement of this study in which novel interpretation has been provided based on assimilating models derived from the freely available data through the project "PESMOS" funded by the Ministry of Earth Sciences, Govt. of India to the Department of Earthquake Engineering, IIT Roorkee.

BS is thankful to Hiroe Miyake, ERI, Tokyo, and T. Yokoi, IISEE, Japan for supporting BS training in Japan availed on sponsorship by JICA on approval by the competent authority of Ministry of Earth Sciences during October 2016 – September 2017. Director, National Centre of Seismology (NCS) is gratefully acknowledged for his encouragement to accomplish this piece of research. Authors express sincere gratitude to Prof. Vernon Cormier, the editor-in-Chief and the two anonymous reviewers whose suggestions and comments significantly improved our manuscript.

References

Bureau of Indian Standards, 2002. IS 1893 (Part I): Indian Standard Criteria for Earthquake Resistant Design of Structures, 5th Revision. Bureau of Indian Standards, New Delhi, India.
Mittal, H., 2011. Estimation of Ground Motion in Delhi. Ph.D. thesis, Dept. of Earthquake Engineering, Indian Institute of Technology, Roorkee, India.
Mittal, H., Kumar, A., 2015. Stochastic finite-fault modeling of Mw5.4 earthquake along Uttarakhand–Nepal border. Nat. Hazards 175, 1145–1166. https://doi.org/10.1007/s11069-014-1367.
Bhatia, S.C., Ravi Kumar, M., Gupta, H.K., 1999. A probabilistic seismic hazard map of India and adjoining regions. Ann. Geophys. 42, 1153–1166.
Bilham, R., 2004. Earthquakes in India and the Himalaya: tectonics, geodesy and history. Annals of Geophysics 47 (2/3).
Bilham, R., Gaur, V.K., 2000. The geodetic contribution to Indian seismotectonics. Curr. Sci. 79, 2000.
Bilham, R., Wallace, K., 2005. Future Mw 8 earthquake in Himalaya: implication for the 26 December, 2004 M = 9 earthquake on eastern margin. Geol. Surv. India 85, 1–14.
Bilham, R., Gaur, V.K., Molnar, P., 2001. Himalayan seismic hazard. Science 293, 1442–1444.
De, R., Kayal, J.R., 2003. Seismotectonic model of the Sikkim Himalaya: constraint from micro earthquake surveys. Bull. Seismol. Soc. Am. 93, 1395–1400.
De, R., Kayal, J.R., 2004. Seismic activity at the MCT in Sikkim Himalaya. Tectonophysics 386, 243–248.
Diehl, T., Kraft, T., Kissling, E., Wiemer, S., 2017. The induced earthquake sequence related to the St. Gallen deep geothermal project (Switzerland): fault reactivation and fluid interactions imaged by microseismicity. J. Geophys. Res. Solid Earth. https://doi.org/10.1002/2017 JB014473.
Dinesh, Kumar, Khattri, K.N., Teotia, S.S., Rai, S.S., 1999. Modelling of accelerograms of two Himalayan earthquakes using a novel semi-empirical method and estimation of accelerogram for a hypothetical great earthquake in the Himalaya. Curr. Sci. 76 (6), 819–830.
Dujardin, A., Causse, M., Courboulex, F., Traversa, P., 2016. Simulation of the basin effects in the Po Plain during the Emilia–Romagna seismic sequence (2012) using empirical Green's functions. Pure Appl. Geophys. 173 (6), 1993–2010.
England, P., Houseman, G., 1986. Finite strain calculations of continental deformation comparison with the India-Asia collision zone. J. Geophys. Res. 91, 3664–3676.
Frankel, A., 1995. Simulation strong motions of great earthquakes using recordings of small earthquakes: the Loma Prieta main shock as a test case. Bull. Seismol. Soc. Am. 85, 1144–1160.
Gahalaut, V.K., Kundu, B., Laishram, S.S., Catherine, J., Kumar, A., Devchandra, M., Tiwari, R.P., Samanta, S.K., Ambikapathy, A., Mahesh, P., Bansal, A., Narsaiah, M., 2013. Aseismic plate boundary in the Indo-Burmese wedge, northwest Sunda Arc. Geology 41, 235–238.
Gansser, A., 1964. Geology of the Himalayas, Interscience, New York, vol. 289.
Gupta, H.K., Gahalaut, V.K., 2014. Seismotectonics and large earthquake generation in the Himalayan region. Gondwana Res. 25, 204–213.
Guzman-Speziale, M., Ni, J.F., 1996. Seismicity and Active Tectonics of the Western Sunda Arc. In the Tectonic Evolution of Asia. Cambridge Univ. Press, New York.
Hartzell, S., 1978. Earthquake aftershock as Green's functions. Geophys. Res. Lett. 5, 1–4.
He, P., Lei, J., Yuan, X., Xu, X., 2018. Lateral Moho variations and the geometry of the Main Himalayan Thrust beneath the Nepal Himalayan orogeny revealed by teleseismic receiver functions. Geophys. J. Int. 214, 1004–1017.
Holt, W.E., James, N.F., Wallace, C.T., Haines, A.J., 1991. The active tectonics of the Eastern Himalayan Syntaxis and surrounding regions. J. Geophys. Res. 96 (B9), 14595–14632.
Irikura, K., 1983. Semi-empirical estimation of strong ground motions during large earthquakes. Bull. Disaster Prevention Res. Inst. Kyoto Univ. 32, 63–104.
Irikura, K., 1986. Prediction of strong acceleration motion using empirical Green's function. In: Proc. 7th Japan Earthquake Engineering Symposium, pp. 151–156.
Irikura, K., Miyake, H., 2011. Recipe for predicting strong ground motion from crustal earthquake scenarios. Pure Appl. Geophys. https://doi.org/10.1007/s00024-010-0150-9.
Irikura, K., Kagawa, T., Sekiguchi, H., 1997. Revision of the Empirical Green's function method. Program Abstracts Seismolog. Soc. Jpn 2, B25.
Kamae, K., Irikura, K., Pitarka, A., 1998. A technique for simulating strong ground motion using hybrid Green's function. Bull. Seismol. Soc. Am. 88, 357–367.
Kayal, J.R., 2008. Micro Earthquake Seismology and Seismotectonics of South Asia. Springer, Heidelberg, Germany.
Kayal, J.R., De, R., Charkraborty, P., 1993. Micro earthquakes at the main boundary thrust in eastern Himalaya and the present day tectonic model. Tectonophysics 218, 375–381.
Kayal, J.R., Arefiev, S.S., Baruah, S., Tatevossian, R., Gogoi, N., Sanoujam, M., Gautam, J.L., Hazarika, D., Borah, D., 2010. The 2009 Bhutan and Assam felt earthquakes (Mw 6.3 and 5.1) at the Kopili fault in the northeast Himalaya region. Geomat. Nat. Haz. Risk. 1, 273–281.
Khattri, K.N., 1992. Local seismic investigations in the Garhwal-Kumaon Himalaya. Mem. Geol. Soc. India 23, 275–302.
Khattri, K.N., 1999. An evaluation of earthquakes hazards and risk in northern India. Himal. Geol. 20, 1–46.
Khattri, K.N., Rogers, A.M., Algermissen, S.T., 1984. A seismic hazard map of India and adjacent areas. Tectonophys 108, 93–134.
Khattri, K.N., Chander, R., Gaur, V.K., Sarkar, I., Kumar, S., 1989. New seismological results on the tectonics of the Garhwal Himalaya. Proc. Indian Acad. Sci. Earth Planet. 98, 91–109.
Kumar, A., Mittal, H., Sachdeva, R., Kumar, A., 2012. Indian national strong motion network. Seismol. Res. Lett. 83 (1), 29–36.
Kumar, A., Kumar, A., Gupta, S.C., Mittal, H., Kumar, R., 2013. Source parameters and fmax in Kameng region of Arunachal Lesser Himalaya. J. Asian Earth Sci. 70, 35–44.
Kumar, R., Gupta, S.C., Kumar, A., Mittal, H., 2015. Source parameters and f_{max} in lower Siang region of Arunachal lesser Himalaya. Arab. J. Geosci. 8 (1), 255–265.
Kumar, A., Mittal, H., Kumar, R., Ahluwalia, R.S., 2017. Empirical attenuation relationship for peak ground horizontal acceleration for North-East Himalaya. Vietnam J. Earth Sci. 39 (1), 47–57.
Kundu, B., Gahalaut, V.K., 2012. Earthquake occurrence process in the Indo-Burmese wedge and Sagaing fault region. Tectonophysics 524–525, 135–146.
Le Dain, A.Y., Tapponier, P., Molnar, P., 1984. Active faulting and tectonics of Burma and surrounding regions. J. Geophys. Res. 89, 453–472.
Le Roux-Mallouf, R., Godard, V., Cattin, R., Ferry, M., Gyeltshen, J., Ritz, J.F., Drupka, D., Guillou, V., Arnold, M., Aumaître, G., Bourlès, D.L., Keddadouche, K., 2015. Evidence for a wide and gently dipping Main Himalayan Thrust in western Bhutan. Geophys. Res. Lett. 42 https://doi.org/10.1002/2015GL063767.
Le Roux-Mallouf, R., Ferry, M., Ritz, J.F., Berthet, T., Cattin, R., Drukpa, D., 2016. First paleoseismic evidence for great surface-rupturing earthquakes in the Bhutan Himalayas. J. Geophys. Res. Solid Earth 121. https://doi.org/10.1002/2015JB012733.
Lei, J., Zhao, D., 2016. Teleseismic P-wave tomography and mantle dynamics beneath Eastern Tibet. Geochem. Geophys. Geosyst. 17, 1861–1884.
Lei, J., Zhao, D., Su, Y., 2009. Insight into the origin of the Tengchong intraplate volcano and seismotectonics in southwest China from local and teleseismic data. J. Geophys. Res. 114, B05302 https://doi.org/10.1029/2008JB005881.
Lei, J., Zhao, D., Xu, X., Xu, Y., Du, M., 2019. Is there a big mantle wedge under eastern Tibet? Phys. Earth Planet. Inter. 292, 100–113.
Mahajan, A.K., Thakur, V.C., Sharma, M.L., Chauhan, M., 2010. Probabilistic Seismic Hazard map of NW Himalaya and its adjoining area. Nat. Hazards 53, 443–457.
Mishra, O.P., 2011. Three - Dimensional Tomography of Northeast India and Indo - Burma Region and its implications for Earthquake Risks, National Workshop on Earthquake Risk Mitigation Strategy in North East India, NIDM, pp. 40–54.
Mishra, O.P., 2012. Seismological research in India (2007 – 2011). Proceeds. Ind. Nat. Sci. Acad. Publication (PINSA) 76 (3), 361–375.

Mishra, O.P., 2014. Intricacies of the Himalayan seismotectonics and seismogenesis: for integrated research. Curr. Sci. 106 (2), 176–187.
Mishra, O.P., 2020. Seismic microzonation study of South Asian cities and its implications to Urban risk resiliency under Climate Change Scenario. Int. J. Geosci. 11 (4), 197–237. https://doi.org/10.4236/ijg.2020.114012.
Mishra, O.P., Vandana, Gera, Sasi K., Kumar, Vikas, 2020a. A new insight into seismic attenuation characteristics of Northwest Himalaya and its surrounding regions: implications to structural heterogeneities and earthquake hazards. Phys. Earth Planet. Inter. https://doi.org/10.1016/j.pepi.2020.106500.
Mishra, O.P., Priya, Singh, Ram, B., Gera, Sasi Kiran, Singh, O.P., Mukherjee, K.K., Chakrabortty, G.K., Chandrasekhar, S.V.N., Selinraj, A., Som, S.K., 2020b. Seismic site specific study for seismic microzonation: a way forward for risk resiliency of vital infrastructure in Sikkim, India. Int. J. Geosci. 11 (3), 125–144. https://doi.org/10.4236/ijg.2020.113008.
Mittal, H., Kumar, A., Ramhmachhuani, R., 2012. Indian national strong motion instrumentation network and site characterization of its stations. Int. J. Geosci. 03, 1151–1167. https://doi.org/10.4236/ijg.2012.326117.
Mittal, H., Gupta, S., Srivastava, A., Dubey, R.N., Kumar, A., 2006. National strong motion instrumentation project: an overview. In: 13th Symposium on Earthquake Engineering. Indian Institute of Technology, Roorkee, Dec 18–20. Elite Publishing, New Delhi, pp. 107–115.
Miyake, H., Iwata, T., Irikura, K., 2003. Source characterization for broadband ground-motion simulation: kinematic heterogeneous source model and strong motion generation area. Bull. Seismol. Soc. Am. 93, 2531–2545.
Molnar, P., Chen, W.P., 1982. Seismicity and mountain building. In: Hsu, K. (Ed.), Mountain Building Processes. Academic, New York, pp. 41–57.
Motazedian, D., Atkinson, G.M., 2005. Stochastic finite-fault modeling based on dynamic corner frequency. Bull. Seismol. Soc. Am. 95, 995–1010.
Nath, S.K., Thingbaijam, K.K.S., 2012. Probabilistic seismic hazard assessment of India. Seismol. Res. Lett. 83 (1), 135–149.
Nath, S.K., Thingbaijam, K.K.S., Raj, A., 2008. Earthquake hazard in the Northeast India – a seismic microzonation approach with typical case studies from Sikkim Himalaya and Guwahati city. J. Earth. Sys. Sci. 117, 809–831.
Oldham, R.D., 1899. Report on the great earthquake of 12th June, 1897. Geolog. Sur. India Publ. Memoir. 29, 379.
Ordaz, M., Arboleda, J., Singh, S.K., 1995. A scheme of random summation of an empirical Green's function to estimate ground motions from future large earthquakes. Bull. Seismol. Soc. Am. 85, 1635–1647.
Parvez, I.A., Vaccari, F., Panza, G.F., 2003. A deterministic seismic hazard map of India and adjacent areas. Geophys. J. Int. 155, 489–508.
Sandhu, M., Sharma, B., Mittal, H., Chingtham, P., 2020. Analysis of the site effects in the north east region of India using the recorded strong ground motions from moderate earthquakes. J. Earthq. Eng. 1-20.
Searle, M.P., Windley, B.F., Coward, M.P., Cooper, M.P., Rex, A.J., Rex, D., Tingdong, L., Xuchang, X., Jan, M.Q., Thakur, V.C., Kumar, S., 1987. The closing of Tethys and the tectonics of the Himalaya. Bull. Geol. Soc. Am. 98, 678–701.
Seeber, L., Armbruster, J.G., 1981. Great detachment earthquakes along the Himalayan arc and long-term forecasting. In: Earthquake Prediction. An International Review in Maurice Ewing Series 4. American Geophysical Union, Washington, D.C., pp. 259–277
Shaligram, P., Das, J., Kumar, A., Rout, M.M., Das, R., 2014. Probabilistic seismic hazard assessment of Himachal Pradesh and adjoining regions. J. Earth Sys. Sci. 123 (1), 49–62.
Sharma, B., Rastogi, B.K., 2014. Spatial distribution of scatterers in the crust of Kachchh region, Western India by inversion analysis of coda envelopes. Disaster Adv. 7 (5), 84–93.
Sharma, M.L., Douglas, J., Bungum, H., Kotadia, J., 2009. Ground-motion prediction equations based on data from the Himalayan and Zagros Regions. J. Earthq. Eng. 13, 1191–1210.
Sharma, B., Chopra, S., Sutar, A.K., Bansal, B.K., 2013. Estimation of strong ground motion from a great earthquake in central seismic gap region using empirical green's function method. Pure Appl. Geophys. https://doi.org/10.1007/s00024-013-0647-0.
Sharma, B., Chingtham, P., Sutar, A.K., Chopra, S., Shukla, H.P., 2015. Frequency dependent attenuation of seismic waves for Delhi and surrounding area, India. Ann. Geophys. 58 (2) https://doi.org/10.4401/ag-6636.
Sharma, B., Chopra, S., Chingtham, P., Kumar, V., 2016a. A study of characteristics of ground motion response spectra from earthquakes recorded in NE Himalayan region: an active plate boundary. Nat. Hazards. https://doi.org/10.1007/s11069-016-2543-2.
Sharma, B., Chopra, S., Kumar, V., 2016b. Simulation of strong ground motion for 1905 Kangra earthquake and a possible mega thrust earthquake (Mw 8.5) in western Himalaya (India) using Empirical Green's Function technique. Nat. Hazards 80 (1), 487–503.
Sharma, B., Chingtham, P., Sharma, V., Kumar, V., Mandal, H.S., Mishra, O.P., 2017. Characteristic ground motions of the 25th April 2015 Nepal earthquake (Mw 7.9) and its implications for the structural design codes for the border areas of India to Nepal. J. Asian Earth Sci. 133, 12–23.
Singh, S.K., Mohanty, W.K., Bansal, B.K., Roonwal, G.S., 2002. Ground motion in Delhi from future large/great earthquakes in the central seismic gap of the Himalayan arc. Bull. Seismol. Soc. Am. 92 (2), 555–569.
Sitharam, T.G., Kolathayar, S., James, N., 2015. Probabilistic assessment of surface level seismic hazard in India using topographic gradient as a proxy for site condition. Geosci. Front. 6, 847–859.
Somerville, P.G., Irikura, K., Graves, R., Sawada, S., Wald, D., Abrahamson, N., Iwasaki, Y., Kagawa, T., Smith, N., Kowada, A., 1999. Characterizing earthquake slip models for the prediction of strong ground motion. Seismol. Res. Lett. 70, 59–80.
Sriram, V., Khattri, K.N., 1999. Modelling of strong ground motions from Dharmsala earthquake of 1986 (mb 5.7). Curr. Sci. 76 (3), 429–438.
Srivastava, H.N., Verma, M., Bansal, B.K., 2010. Seismological constraints for the 1905 Kangra earthquake and associated hazard in Northwest India. Curr. Sci. 99 (11), 1549–1559.
Steckler, M.S., Ranjan Mondal, D., Akhter, S.H., Seeber, L., Jonathan Gale, L.F., Hill, E. M., Howe, M., 2016. Locked and loading megathrust linked to active subduction beneath the Indo-Burman ranges. Nat. Geosci. https://doi.org/10.1038/NGEO2760.
Sutar, A.K., Verma, M., Pandey, A.P., Bansal, B.K., Prasad, P.R., Rao, P.R., Sharma, B., 2017. Assessment of maximum earthquake potential of the Kopili fault zone in Northeast India and strong ground motion simulation. J. Asian Earth Sci. 147, 439–451.
Tandon, A.N., 1954. Study of the great Assam earthquake of Aug. 15, 1950 and its aftershocks. Indian J. Meteorol. 5, 95–137.
Tapponnier, P., et al., 1981. The Tibetan side of the India-Eurasian collision. Nature 294, 405–410.
Tapponnier, P., et al., 1990. The Ailao Shan/Red-River metamorphic belt: tertiary left-lateral shear between Indochina and South China. Nature 343, 431–437.
Thingbaijam, K.K.S., Nath, S.K., Yadav, A., 2008. Recent seismicity in Northeast India and its adjoining region. J. Seismol. 12, 107–123.
Valdiya, K.S., 1988. Dynamic Himalaya. Universities Press, Hyderabad.
Wang, Y., Sieh, K., Tun, S.T., Lai, K., Myint, T., 2014. Active tectonics and earthquake potential of the Myanmar region. J. Geophys. Res. 119, 3767–3822.
Yin, A., Harrison, T., 2000. Geological evolution of the Himalayan-Tibetan orogen. Annu. Rev. Earth Planet. Sci. 28, 211–280.
Zhou, Z., Lei, J., 2016. Pn anisotropic tomography and mantle dynamics beneath China. Phys. Earth Planet. Inter. 257, 193–204.